Detection, Estimation, and Modulation Theory, Part III: Radar–Sonar Signal Processing and Gaussian Signals in Noise. Harry L. Van Trees

ISBNs: 0-471-10793-X (Paperback); 0-471-22109-0 (Electronic)

10

Parameter Estimation: Slowly Fluctuating Point Targets

At the beginning of Chapter 9, we developed a model for the return from a slowly fluctuating point target that was located at a particular range and was moving at a particular velocity. The received signal in the absence of noise was

$$s(t) = \sqrt{2}\,\mathrm{Re}\,[\sqrt{E_t}\,\tilde{b}\tilde{f}(t-\tau)e^{j\omega_D t}]. \tag{1}$$

In the detection problem we assumed that τ and ω_D were known, and made a decision on the presence or absence of a target. We now consider the problem in which τ and ω_D are *unknown*, *nonrandom* parameters that we want to estimate.

Since the chapter is long, we briefly describe its organization. In Section 10.1 we derive the optimum receiver and discuss signal design qualitatively. In Section 10.2 we analyze the performance of the optimum receiver. We find that a function called the ambiguity function plays a central role in the performance discussion. In Section 10.3 we develop a number of properties of this function, which serve as a foundation for the signal design problem. In Section 10.4 we investigate the performance of coded pulse sequences. In Section 10.5 we consider the situation in which there are interfering targets in addition to the desired target whose parameters we want to estimate. Finally, in Section 10.6, we summarize our results and discuss several related topics.

10.1 RECEIVER DERIVATION AND SIGNAL DESIGN

The target reflection model was discussed in Section 9.1, and the received signal in the absence of noise is given in (1). We assume that the additive noise is white bandpass Gaussian noise with spectral height

$N_0/2$. We shall assume that the observation interval is infinite. For notational simplicity we drop the subscript D from the frequency shift. Thus, the complex envelope of the received waveform is

$$\tilde{r}(t) = \tilde{b}\sqrt{E_t}\tilde{f}(t-\tau)e^{j\omega t} + \tilde{w}(t), \qquad -\infty < t < \infty. \tag{2}$$

The multiplier, $\tilde{b}$, is a zero-mean complex Gaussian random variable,

$$E[|\tilde{b}|^2] = 2\sigma_b^2. \tag{3}$$

The complex signal envelope is normalized as in (A.15), so that E_t is the transmitted energy. The average received signal energy is

$$\bar{E}_r = 2\sigma_b^2 E_t. \tag{4}$$

The complex white noise has a covariance function

$$\tilde{K}_{\tilde{w}}(t, u) = N_0\,\delta(t-u), \qquad -\infty < t, u < \infty. \tag{5}$$

The parameters τ and ω are unknown nonrandom parameters whose values we shall estimate.

The first step is to find the likelihood function. Recalling from Chapter I-4 the one-to-one correspondence between the likelihood function and the likelihood ratio, we may use (9.36), (9.38), and (9.39) to obtain the answer directly. The result is

$$\ln \Lambda_1(\tau, \omega) = \frac{1}{N_0}\frac{\bar{E}_r}{N_0 + \bar{E}_r}\{|\tilde{L}(\tau, \omega)|^2\}, \tag{6}$$

where

$$\tilde{L}(\tau, \omega) = \int_{-\infty}^{\infty} \tilde{r}(t)\tilde{f}^*(t-\tau)e^{-j\omega t}\,dt. \tag{7}$$

The coefficient in (6) is of importance only when we compute the Cramér-Rao bound, and we can suppress it in most of our discussion. Then we want to compute

$$\ln \Lambda(\tau, \omega) = |\tilde{L}(\tau, \omega)|^2 \tag{8}$$

as a function of τ and ω. The values of τ and ω where this function has its maximum are $\hat{\tau}_{ml}$ and $\hat{\omega}_{ml}$. Because we are considering only maximum likelihood estimates, we eliminate the subscript in subsequent expressions.

We now must generate $\ln \Lambda(\tau, \omega)$ for the values of τ and ω in the region of interest. For any particular ω, say ω_1, we can generate $\ln \Lambda(\tau, \omega_1)$ as a function of time by using a bandpass matched filter and square-law envelope detector (recall Fig. 9.5). For different values of ω we must use different filters. By choosing a set of ω_i that span the frequency range of interest, we can obtain a discrete approximation to $\ln \Lambda(\tau, \omega)$. For the moment we shall not worry about how fine the frequency grid must be in

order to obtain a satisfactory approximation. The processing system is a bank of matched filters and square-law envelope detectors as shown in Fig. 10.1. We now want to investigate the properties of the output of the processor. For simplicity, we view it as a continuous function of τ and ω.

Let us assume that the actual delay and Doppler shift are τ_a and ω_a, respectively. (Recall that τ and ω are the variables in the likelihood function.) Then we may write

$$\begin{aligned}\tilde{L}(\tau, \omega) &= \int_{-\infty}^{\infty} \tilde{r}(t)\tilde{f}^*(t-\tau)e^{-j\omega t}\,dt \\ &= \int_{-\infty}^{\infty} [\sqrt{E_t}\,\tilde{b}\tilde{f}(t-\tau_a)e^{j\omega_a t} + \tilde{w}(t)][\tilde{f}^*(t-\tau)e^{-j\omega t}]\,dt, \qquad (9)\end{aligned}$$

or

$$\begin{aligned}\tilde{L}(\tau, \omega) = \sqrt{E_t}\,\tilde{b}\int_{-\infty}^{\infty} \tilde{f}(t-\tau_a)\tilde{f}^*(t-\tau)e^{j(\omega_a-\omega)t}\,dt \\ + \int_{-\infty}^{\infty} \tilde{w}(t)\tilde{f}^*(t-\tau)^{-j\omega t}\,dt. \qquad (10)\end{aligned}$$

To simplify this expression we define

$$\tau' = \tau - \tau_a, \qquad (11)$$

$$\omega' = \omega - \omega_a, \qquad (12)$$

and

$$\tilde{n}(\tau, \omega) = \int_{-\infty}^{\infty} \tilde{w}(t)\tilde{f}^*(t-\tau)e^{-j\omega t}\,dt. \qquad (13)$$

The effect of (11) and (12) is to shift the origin to the point in the τ, ω plane where the target is located. This is shown in Fig. 10.2. Using (11)–(13) in (10), we have

$$\begin{aligned}\ln \Lambda(\tau, \omega) = E_t|\tilde{b}|^2 \left\{\left|\int_{-\infty}^{\infty} \tilde{f}(t-\tau)\tilde{f}^*(t-\tau+\tau')e^{j\omega' t}\,dt\right|^2\right\} \\ + 2\,\mathrm{Re}\left\{\sqrt{E_t}\,\tilde{b}\left(\int_{-\infty}^{\infty} \tilde{f}^*(t-\tau)\tilde{f}(t-\tau+\tau')e^{-j\omega' t}\,dt\right)\tilde{n}^*(\tau, \omega)\right\} \\ + |\tilde{n}(\tau, \omega)|^2. \qquad (14)\end{aligned}$$

The first term in (14) is due entirely to the signal and is the only term that would be present in the absence of noise. By making the substitution

$$z = t - \tau + \frac{\tau'}{2}, \qquad (15)$$

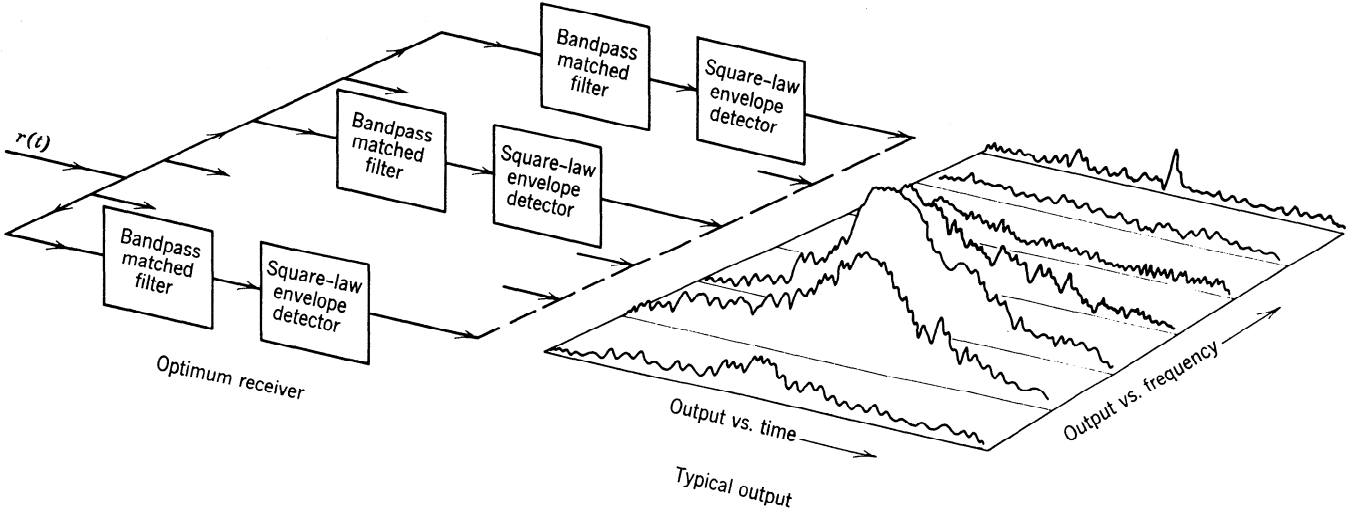

Fig. 10.1 Receiver to generate ln Λ (τ, ω).

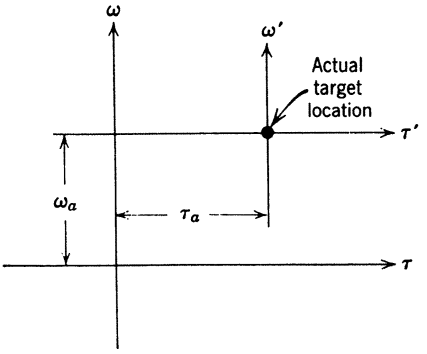

Fig. 10.2 Coordinate systems in the τ, ω plane.

we see that it is not a function of τ and ω. We denote the term in braces as $\theta(\tau', \omega')$,

$$\theta(\tau', \omega') \triangleq \left| \int_{-\infty}^{\infty} \tilde{f}\left(z - \frac{\tau'}{2}\right) \tilde{f}^*\left(z + \frac{\tau'}{2}\right) e^{j\omega' z}\, dz \right|^2. \tag{16}$$

It corresponds to a scaled (by $E_t\,|\tilde{b}|^2$) version of the output of the receiver in the absence of noise.

We define the function inside the magnitude signs as the *time-frequency autocorrelation function* of $\tilde{f}(t)$ and denote it by $\phi(\tau', \omega')$,†

$$\boxed{\phi(\tau', \omega') \triangleq \int_{-\infty}^{\infty} \tilde{f}\left(t - \frac{\tau'}{2}\right) \tilde{f}^*\left(t + \frac{\tau'}{2}\right) e^{j\omega' t}\, dt.} \tag{17}$$

It is a measure of the degree of similarity between a complex envelope and a replica of it that is shifted in time and frequency. Clearly,

$$\boxed{\theta(\tau', \omega') = |\tilde{\phi}(\tau', \omega')|^2.} \tag{18}$$

The function $\theta(\tau', \omega')$ was introduced originally by Ville [1] and is referred to as the *ambiguity function.* Later we shall see why this is an appropriate name. It is sometimes referred to as Woodward's ambiguity function because of his pioneering work with it [8], [60].

Because $\tilde{f}(t)$ is normalized it follows that

$$\phi(0, 0) = 1. \tag{19}$$

From the Schwarz inequality,

$$|\phi(\tau', \omega')| \leq \phi(0, 0) = 1 \tag{20}$$

† There is a certain degree of choice in defining the time-frequency autocorrelation function, and various definitions are used in the literature.

and

$$\theta(\tau', \omega') \leq \theta(0, 0) = 1. \tag{21}$$

Thus, the output of the receiver is a surface in the τ, ω plane that contains three components. The first is $\theta(\tau', \omega')$, which is a positive function whose maximum value is at that point in the plane where the target is located. The second and third terms are due to the additive noise. In a moment, we shall consider the effect of these two terms, but first we look at $\theta(\tau', \omega')$ in more detail.

To get some feeling for the behavior of $\theta(\tau, \omega)$ and $\phi(\tau, \omega)$ for some typical signals, we consider several examples.

Example 1. Single Rectangular Pulse. Let $\tilde{f}(t)$ be a real rectangular pulse,

$$\tilde{f}(t) = \begin{cases} \dfrac{1}{\sqrt{T}}, & -\dfrac{T}{2} < t < \dfrac{T}{2}, \\ 0, & \text{elsewhere.} \end{cases} \tag{22}$$

Then

$$\phi(\tau, \omega) = \begin{cases} \dfrac{1}{T} \displaystyle\int_{-\frac{1}{2}(T-|\tau|)}^{\frac{1}{2}(T-|\tau|)} e^{j\omega t}\, dt = \left(1 - \frac{|\tau|}{T}\right)\left(\frac{\sin\left[(\omega T/2)(1 - (|\tau|/T))\right]}{(\omega T/2)(1 - (|\tau|/T))}\right), & \tau \leq T, \\ 0, & \text{elsewhere,} \end{cases} \tag{23}$$

and

$$\theta(\tau, \omega) = \begin{cases} \left(1 - \dfrac{|\tau|}{T}\right)^2 \left(\dfrac{\sin\left[(\omega T/2)(1 - (|\tau|/T))\right]}{(\omega T/2)(1 - (|\tau|/T))}\right)^2, & |\tau| \leq T, \\ 0, & \text{elsewhere.} \end{cases} \tag{24}$$

The magnitude of the time-frequency autocorrelation function is shown in Fig. 10.3. (Actually we show some cuts through the surface along constant τ and constant ω lines.) Notice that the function is symmetric about both axes.

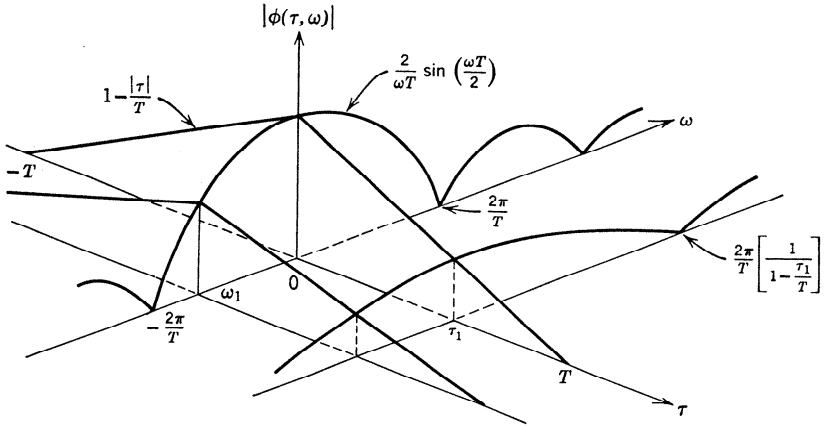

Fig. 10.3 Magnitude of the time-frequency correlation function for a rectangular pulse.

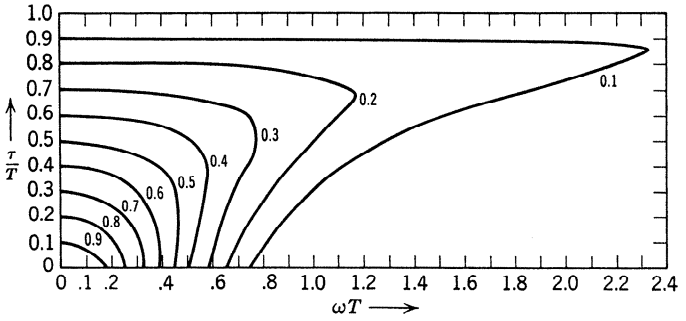

Fig. 10.4 Equal-height contours of ambiguity function of rectangular pulse.

A convenient method of representing the ambiguity function is shown in Fig. 10.4. The curves are equal-height contours of $\theta(\tau, \omega)$. Notice that the τ-axis and ω-axis are scaled by factors of T^{-1} and T, respectively. Notice also that the ambiguity function has a single peak whose width along the τ-axis is *directly* proportional to T and whose width along the ω-axis is *inversely* proportional to T.

Before considering a second example it is worthwhile discussing *qualitatively* how the other two terms in (14) affect the estimate of τ and ω in a typical realization of the experiment. In order to see this, we first consider a vertical cut along the τ-axis of $\ln \Lambda(\tau, \omega)$ as shown in Fig. 10.5*a*. From (14) we see that the function consists of $E_t |\tilde{b}|^2 \theta(\tau, 0)$ plus the contributions due to noise indicated by the second and third terms. In Fig. 10.5*b*, we show a top view of $\ln \Lambda(\tau, \omega)$. The shaded surface is the $E_t |\tilde{b}|^2 \theta(\tau, \omega)$ from Fig. 10.4. The contour lines are the equal-height loci of $\ln \Lambda(\tau, \omega)$. The values of τ and ω where the surface has its maximum are $\hat{\tau}_{ml}$ and $\hat{\omega}_{ml}$. We see that in the absence of noise we always choose the correct values. There will be an error if the noise contributions at some $\tau' \neq 0$ and $\omega' \neq 0$ are large enough to move the peak of the total function away from the origin. Therefore, in order to minimize the errors, we should try to find an $\tilde{f}(t)$ whose ambiguity function is one at the origin and zero elsewhere. An *ideal* $\theta(\tau, \omega)$ function might be the one shown in Fig. 10.6*a*. We expect that it will be difficult to find an $\tilde{f}(t)$ that has such a discontinuous ambiguity function. However, a close approximation such as is shown in Fig. 10.6*b might* be practical.

Thus, it appears that we want to choose $\tilde{f}(t)$ so that $\theta(\tau, \omega)$ is a narrow spike. From (24) or Fig. 10.3, it is clear that, with a rectangular pulse, we can make the peak arbitrarily narrow in either direction (but *not* both) by varying T.

Since the rectangular pulse does not lead to the ambiguity function in Fig. 10.6*b*, we shall try some other signals.

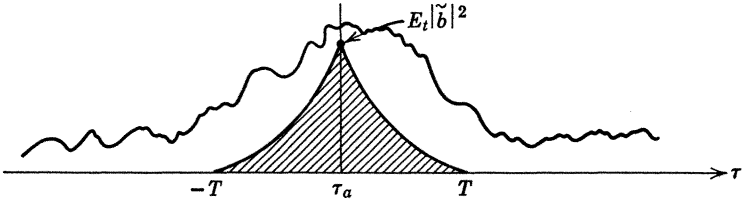

(a) Cut of $\ln \Lambda\ (0, \omega)$

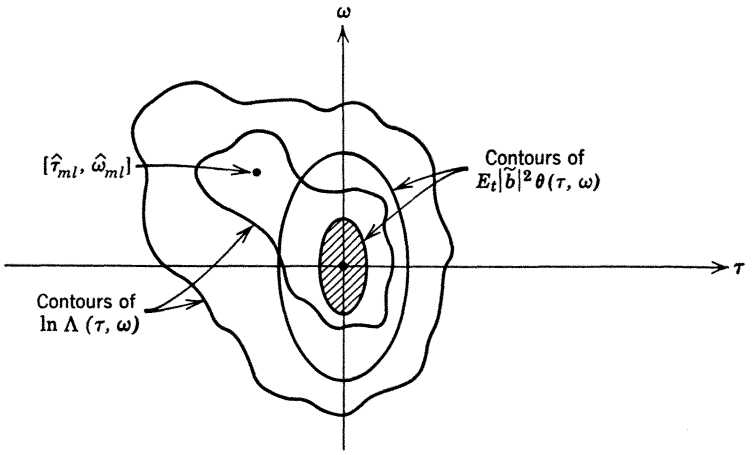

(b) Contours of typical output

Fig. 10.5 Output of receiver on a particular experiment.

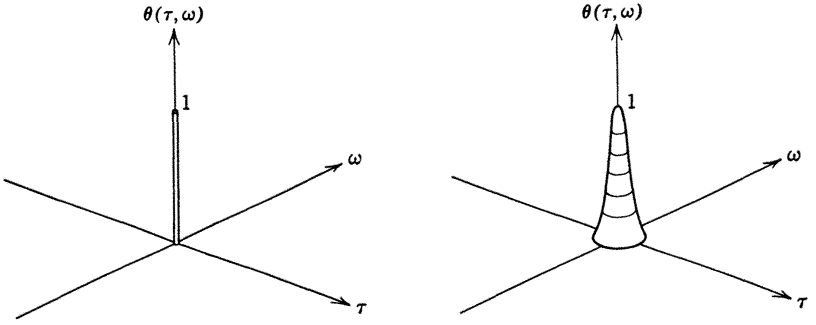

(a) Ideal ambiguity function

(b) Possible approximation to ideal ambiguity function

Fig. 10.6 Desirable ambiguity functions.

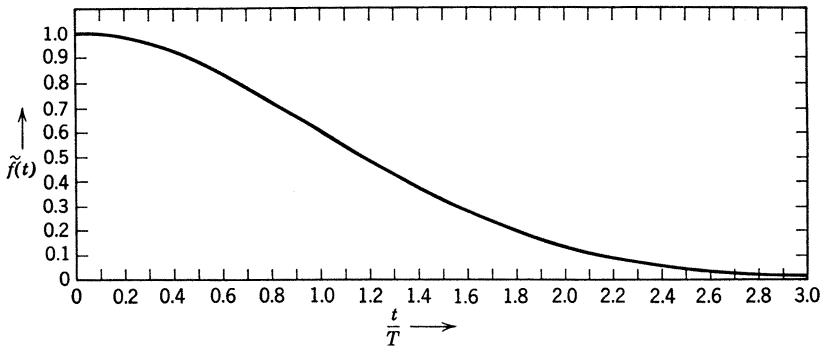

Fig. 10.7 Gaussian pulse.

Example 2. Simple Gaussian Pulse. A pulse that frequently serves as a useful analytic idealization is the Gaussian pulse of Fig. 10.7.

$$\tilde{f}(t) = \left(\frac{1}{\pi T^2}\right)^{1/4} \exp\left(-\frac{t^2}{2T^2}\right), \qquad -\infty < t < \infty. \tag{25}$$

The effective duration is proportional to T. The time-frequency autocorrelation function is

$$\phi(\tau, \omega) = \int_{-\infty}^{\infty} \left(\frac{1}{\pi T^2}\right)^{1/4} \exp\left[-\frac{(t-\tau/2)^2}{2T^2} - \frac{(t+\tau/2)^2}{2T^2} + j\omega t\right]. \tag{26}$$

Completing the square and integrating, we obtain

$$\phi(\tau, \omega) = \exp\left[-\tfrac{1}{4}\left(\frac{\tau^2}{T^2} + T^2\omega^2\right)\right]. \tag{27}$$

The ambiguity function is

$$\theta(\tau, \omega) = \exp\left[-\tfrac{1}{2}\left(\frac{\tau^2}{T^2} + T^2\omega^2\right)\right]. \tag{28}$$

The equal-height contours of $\theta(\tau, \omega)$ are ellipses, as shown in Fig. 10.8. Just as in Example 1, a single parameter, the pulse duration, controls both the range and Doppler accuracy.

These two examples suggest that if we are going to improve our range and Doppler estimates *simultaneously*, we must try a more complicated signal. Apparently, we need a signal that contains several parameters which we can vary to optimize the performance. We shall consider two broad classes of signals.

Coded Pulse Sequences. This class of signals is constructed by operations on single subpulse, $\tilde{u}(t)$. A commonly used subpulse is the rectangular

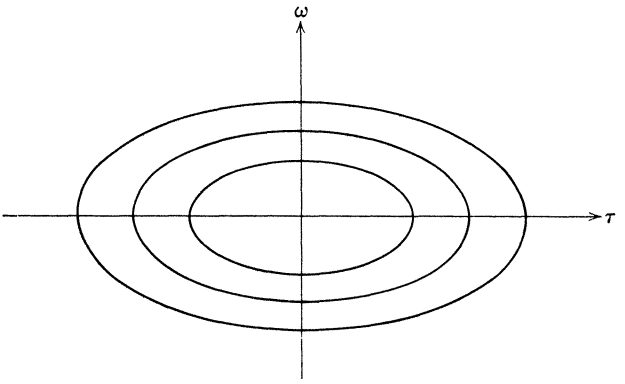

(a) $T = \sqrt{2}$

Fig. 10.8 Equal-height contours for the ambiguity function of a Gaussian pulse with $T = \sqrt{2}$.

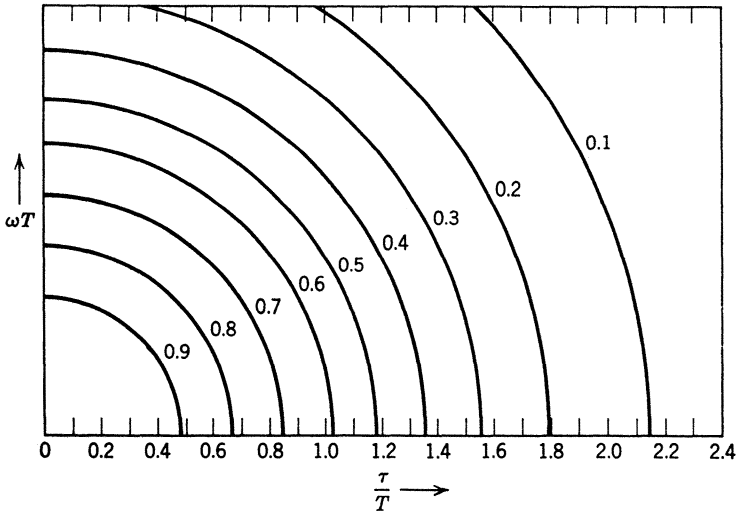

(b) Normalized axes

Fig. 10.8 Equal-height contours for ambiguity function of Gaussian pulse (normalized axes).

pulse in Example 1,

$$\tilde{u}(t) = \begin{cases} \dfrac{1}{\sqrt{T}}, & -\dfrac{T}{2} \leq t \leq \dfrac{T}{2}, \\ 0, & \text{elsewhere.} \end{cases} \tag{29}$$

The subpulses are delayed, amplitude-weighted, frequency-shifted, phase-shifted, and then summed. Thus,

$$\tilde{f}(t) = c \sum_{n=1}^{N} \tilde{a}_n \tilde{u}(t - nT) \exp\left[j(\omega_n t + \theta_n)\right]. \tag{30}$$

The constant c normalizes $\tilde{f}(t)$. We discuss a simple example of this class of signal in Example 3. In Section 10.4, we study the class in detail.

Modulated Analog Waveforms. This class is obtained by modulating the signal in amplitude and/or frequency to achieve the desired properties. A simple example of this class of signals is given in Examples 4 and 5.

We now derive the ambiguity function for several useful signals. These examples give us some feeling for the general properties that we might expect.

Example 3. Pulse Train with Constant Repetition Rate. Consider the sequence of rectangular pulses shown in Fig. 10.9. It is characterized by the pulse duration T, the interpulse spacing T_p, and the total number of pulses $(2n + 1)$. This sequence is frequently used in radar and sonar systems for the following reasons:

1. It is easy to generate.
2. The optimum receiver is easy to implement.
3. The parameters can be varied to match different operating conditions.

We assume that $T \ll T_p$. The interpulse spacing is not necessarily a multiple of T. The duration of the entire sequence is T_d,

$$T_d \triangleq 2nT_p + T. \tag{31}$$

Denoting the pulse as $\tilde{u}(t)$ [see (29)], we can write the complex envelope of the transmitted signal as

$$\tilde{f}(t) = \frac{1}{(2n+1)T^{1/2}} \sum_{k=-n}^{k=n} \tilde{u}(t - kT_p). \tag{32}$$

Notice that our model assumes that the target does not fluctuate in the T_d seconds during which the signal illuminates it.

We now derive $\phi(\tau, \omega)$ and $\theta(\tau, \omega)$. First, we consider values of $|\tau| < T$. Using (32) in (17) gives

$$\phi(\tau, \omega) = \left(\frac{1}{(2n+1)T}\right) \sum_{k=-n}^{k=n} \int_{kT_p - \frac{1}{2}(T-|\tau|)}^{kT_p + \frac{1}{2}(T-|\tau|)} \tilde{u}\left(t - kT_p - \frac{\tau}{2}\right) \tilde{u}^*\left(t - kT_p + \frac{\tau}{2}\right) \times e^{j\omega t}\, dt \qquad |\tau| \leq |T|. \tag{33}$$

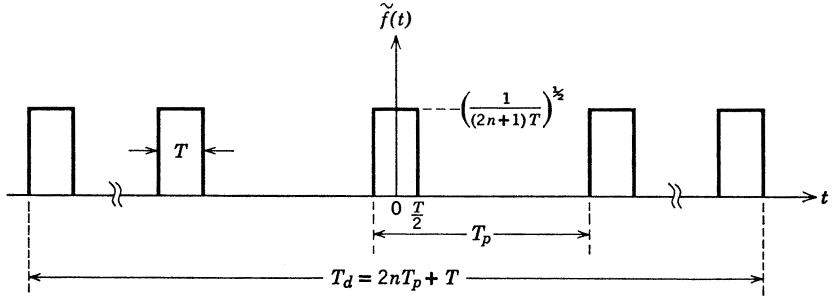

Fig. 10.9 Sequence of pulses.

Letting

$$z = t - kT_p, \tag{34}$$

$$\phi(\tau, \omega) = \left(\frac{1}{(2n+1)T}\right) \sum_{k=-n}^{k=n} e^{j\omega k T_p} \left\{ \int_{-T/2+|\tau|/2}^{T/2-|\tau|/2} \tilde{u}\left(z - \frac{\tau}{2}\right) \tilde{u}^*\left(z + \frac{\tau}{2}\right) e^{j\omega z}\, dz \right\}. \tag{35}$$

The term in the braces is $\phi_{\tilde{u}}(\tau, \omega)$. The sum is a finite geometric series. Thus, (35) reduces to

$$\phi(\tau, \omega) = \frac{1}{(2n+1)} \left\{ \frac{\sin\left[\omega(n + \frac{1}{2})T_p\right]}{\sin\left[\omega T_p/2\right]} \right\} \phi_{\tilde{u}}(\tau, \omega), \qquad |\tau| \leq T. \tag{36}$$

We see that the subpulse characteristics only enter into the last term. The bracketed term is a function of ω only and is determined by T_p, the pulse repetition rate, and n, the number of pulses. The bracketed term is shown in Fig. 10.10*a*. We see that the first zero is at

$$\omega = \frac{2\pi}{(2n+1)T_p} \simeq \frac{2\pi}{T_d}, \tag{37a}$$

and the subsidiary peaks occur at

$$\omega = \frac{2\pi}{T_p}. \tag{37b}$$

In Fig. 10.10*b* we show $\phi_{\tilde{u}}(0, \omega)$ for a rectangular pulse. The two plots indicate the effect of the parameters T, T_p, and T_d. Recalling that

$$T_d > T_p \gg T, \tag{37c}$$

we see that the shape of $\phi(0, \omega)$ is controlled by the term in Fig. 10.10*a*. Thus, the width of the main peak decreases as the over-all duration T_d increases. Subsidary peaks occur at intervals of $1/T_p$ on the frequency axis. When $\omega = 0$, the bracketed term equals $(2n + 1)$, so that

$$\phi(\tau, 0) = \phi_{\tilde{u}}(\tau, 0), \qquad |\tau| \leq T. \tag{38}$$

Next we consider values of $\tau > T$. There is no overlap until $\tau = T_p - T$. At this point, the situation is similar to that at $\tau = -T$, except that there is one less pulse

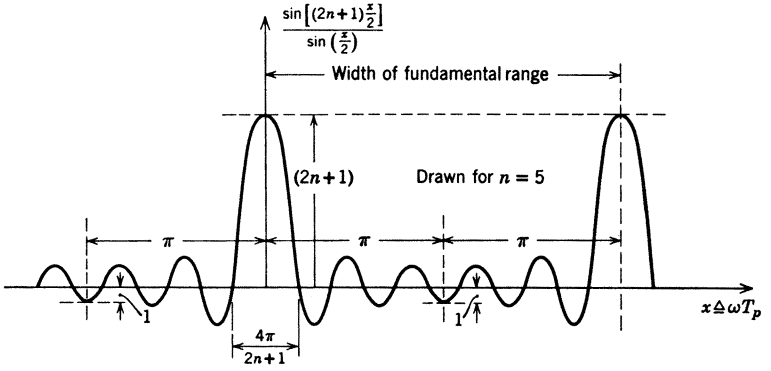

Fig. 10.10*a* **Bracketed term in (36). (After [45].)**

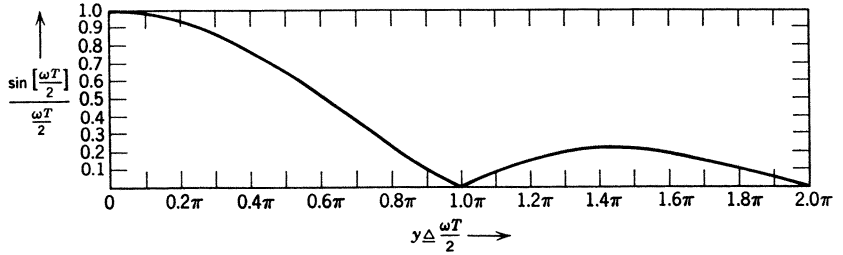

Fig. 10.10*b* **Plot of $|\Phi_{\tilde{u}}(0, \omega)|$ for rectangular pulse.**

overlap. Then, for a rectangular pulse,

$$\phi(\tau, \omega) = \frac{1}{2n+1}\left\{\sum_{k=-n+1}^{n} e^{-j\omega k T_p}\right\}\left\{\frac{\sin\left[\omega(T/2)(1 - |\tau - T_p|/T)\right]}{\omega T/2}\right\}, \qquad |\tau - T_p| \leq T. \tag{39}$$

On the τ-axis we have the same expression as in (38) except for a scale factor and a shift,

$$\phi(\tau, 0) = \left(\frac{2n}{2n+1}\right)\phi_{\tilde{u}}(\tau - T_p, 0), \qquad |\tau - T_p| < T. \tag{40}$$

A similar result follows for larger τ. Every T_p seconds there is a peak, but the magnitude is reduced. A different representation of the ambiguity function $\theta(\tau, \omega)$ is shown in Fig. 10.11. This type of plot was introduced by Siebert [9]. The dark shaded areas indicate regions where the height of $\theta(\tau, \omega)$ is significant (usually, the border corresponds to $\theta(\tau, \omega) = \frac{1}{2}$). In the light shaded areas $\theta(\tau, \omega)$ is small, but nonzero. In the unshaded areas $\theta(\tau, \omega)$ is zero.

Several new features of the signal design problem are indicated by Example 3:

1. We can decrease the width of the major peak in the frequency (Doppler) direction by increasing T_d (or n).

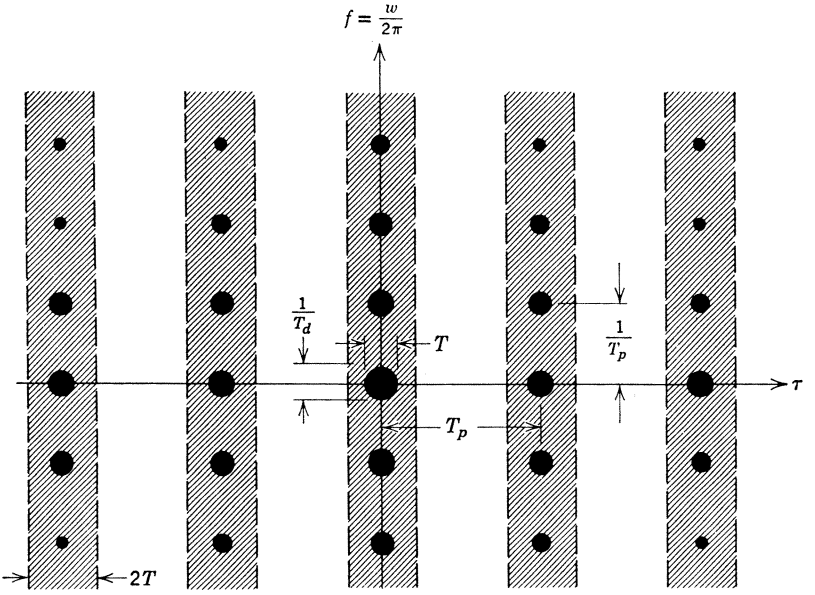

Fig. 10.11 An approximate contour plot of $\theta(\tau, \omega)$ for pulse train [from [9] and [9.12]].

2. We can decrease the width of the major peak in the time (range) direction by decreasing T. (This corresponds to an increased bandwidth.) Thus, by allowing more parameters in our signal design, we can obtain an ambiguity function whose major peak is narrow in both the range and Doppler direction.

3. This particular signal accomplishes this at the cost of including subsidiary peaks. It is easy to see the effects of these subsidiary peaks. A small noise contribution can cause the *total* value at a subsidiary peak to exceed the value at the correct peak. The importance of these subsidiary peaks depends on our a-priori knowledge of the area in the τ,ω plane in which the target may be located. Two cases are shown in Fig. 10.12. In the first case, the set of subsidiary peaks lies outside the area of interest for all possible τ, ω. Thus, they will not cause any trouble. In the second case, they are inside the area of interest, and even in the presence of weak noise we may choose the wrong peak.

This discussion illustrates two of the issues that we encounter in a performance discussion. The first is local accuracy (i.e., given that we are on the correct peak, how small will the error be?). The second is global accuracy (i.e., how often will there be large errors?). This is, of course, the same phenomenon that we encountered in the PFM and PPM problems of Chapter I-4 and in the angle-modulation problems of Chapter II-2.

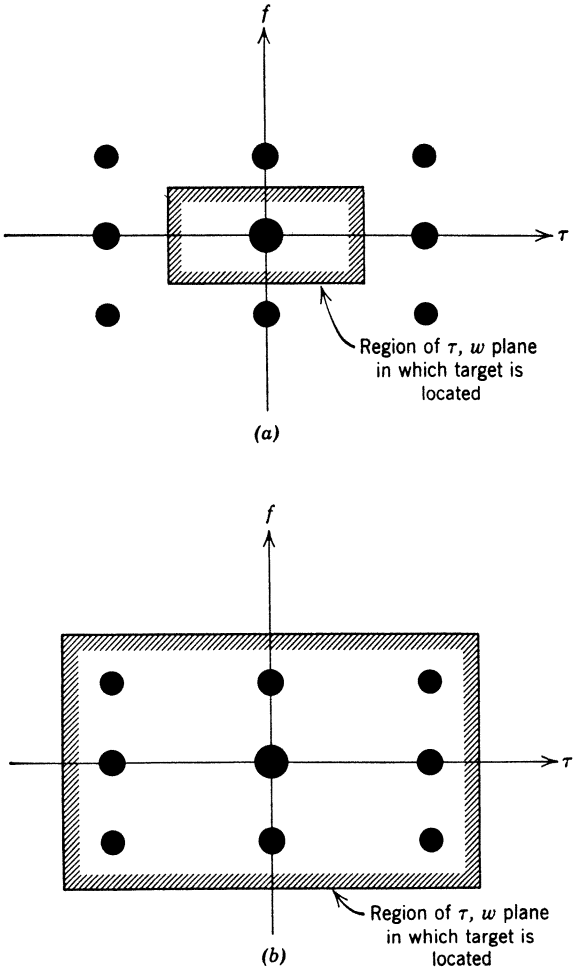

Fig. 10.12 Regions in which target can be located.

Before studying these two issues quantitatively, it is interesting to look at the ambiguity function for several other signals.

We next consider an example of a *modulated analog waveform.* All of our signals up to this point were obtained by amplitude-modulating a constant carrier. In order to introduce more freedom into the signal design, we now consider the possibility of frequency-modulating the carrier. Specifically, we consider a linear frequency sweep, i.e.,

$$\phi_{\tilde{f}}(t) = bt^2. \tag{41}$$

[Recall that $\phi_{\tilde{f}}(t)$ is the phase of $\tilde{f}(t)$.]

Instead of computing the ambiguity function for a particular pulse directly, we use an interesting property for arbitrary $\tilde{f}(t)$.

Property 1. If

$$\tilde{f}_1(t) \sim \phi(\tau, \omega) \sim \theta(\tau, \omega), \tag{42a}$$†

then

$$\tilde{f}_2(t) \triangleq \tilde{f}_1(t)\, e^{jbt^2} \sim \phi(\tau, \omega - 2b\tau) \sim \theta(\tau, \omega - 2b\tau). \tag{42b}$$

This result follows directly from the definitions in (17) and (18).

$$\begin{aligned}
\phi_2(\tau, \omega) &= \int_{-\infty}^{\infty} \tilde{f}_2\left(t - \frac{\tau}{2}\right) \tilde{f}_2^*\left(t + \frac{\tau}{2}\right) e^{j\omega t}\, dt \\
&= \int_{-\infty}^{\infty} \tilde{f}_1\left(t - \frac{\tau}{2}\right) \tilde{f}_1^*\left(t + \frac{\tau}{2}\right) \\
&\quad \times \exp\left[jb\left(t - \frac{\tau}{2}\right)^2 - jb\left(t + \frac{\tau}{2}\right)^2 + j\omega t\right] dt \\
&= \int_{-\infty}^{\infty} \tilde{f}_1\left(t - \frac{\tau}{2}\right) \tilde{f}_1^*\left(t + \frac{\tau}{2}\right) \exp\left[jt[\omega - 2b\tau]\right] dt \\
&= \phi_1(\tau, \omega - 2b\tau).
\end{aligned} \tag{43}$$

Thus, a linear frequency sweep *shears* the ambiguity diagram parallel to the ω-axis. We now apply this property to the Gaussian pulse in Example 2.

Example 4. Gaussian Pulse with Linear Frequency Modulation. Now

$$\tilde{f}(t) = \left(\frac{1}{\pi T^2}\right)^{1/4} \exp\left[-\left(\frac{1}{2T^2} - jb\right)t^2\right]. \tag{44a}$$

Then, from (28) and (42b), we obtain

$$\theta(\tau, \omega) = \exp\left[-\frac{1}{2}\left(\frac{\tau^2}{T^2} + T^2(\omega - 2b\tau)^2\right)\right]. \tag{44b}$$

The equal-height contour lines are the ellipses

$$\frac{1}{2}\left[T^2\omega^2 - 4bT^2\omega\tau + \left(4b^2T^2 + \frac{1}{T^2}\right)\tau^2\right] = c^2. \tag{45}$$

For convenience in plotting, we introduce $\overline{\omega^2}$, $\overline{\omega t}$, and $\overline{t^2}$, which are defined in the Appendix. For the signal in (43),

$$\overline{t^2} = \frac{T^2}{2}, \tag{46}$$

$$\overline{\omega t} = bT^2, \tag{47}$$

† The symbol $\sim$ means "corresponds to."

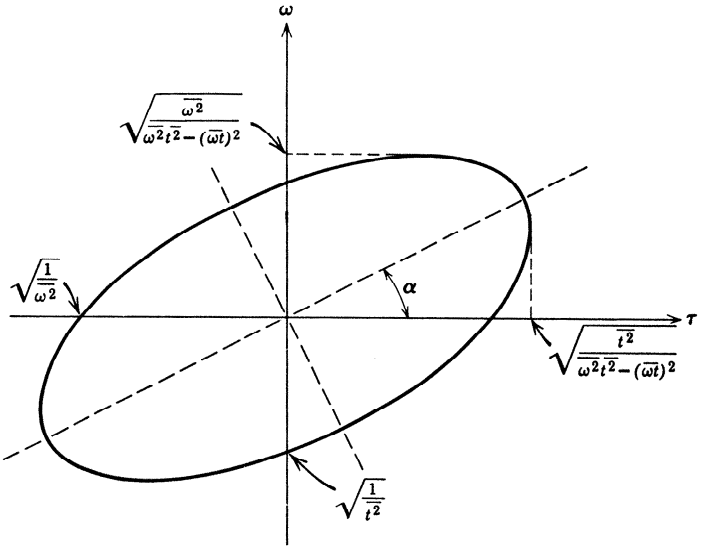

Fig. 10.13 Contour of $\theta(\tau, \omega)$ for Gaussian pulse with linear *FM*.

and

$$\overline{\omega^2} = \frac{1}{2T^2} + 2b^2T^2. \tag{48}$$

Then (45) reduces to

$$\overline{t^2}\omega^2 - 2\overline{\omega t}\omega\tau + \overline{\omega^2}\tau^2 = c^2. \tag{49}$$

In Fig. 10.13 we have plotted (49) for the case when $c = 1$. The major axis is at an angle α, defined by

$$\alpha = \tfrac{1}{2}\tan^{-1}\left(\frac{4b}{1 - (1/4T^4 + b^2)/\pi^2}\right) = \tfrac{1}{2}\tan^{-1}\left(\frac{2\overline{\omega t}}{\overline{t^2} - \overline{\omega^2}/(2\pi)^2}\right), \qquad |\alpha| < \pi. \tag{50}$$

Along the τ-axis,

$$\theta(0, \tau) = \exp\left[-\overline{\omega^2}\tau^2\right] = \exp\left[-\left(\frac{1}{2T^2} + 2b^2T^2\right)t^2\right]. \tag{51a}$$

Similarly,

$$\theta(\omega, 0) = \exp\left[-\overline{t^2}\omega^2\right] = \exp\left[-\frac{T^2\omega^2}{2}\right]. \tag{51b}$$

We see that the width on the τ-axis is inversely proportional to the root-mean-square signal bandwidth and the width on the ω-axis is inversely proportional to the root-mean-square signal duration. Thus, by increasing both b and T, we decrease the width on both the τ- and ω-axes simultaneously. Therefore, we can accurately measure the range of a target with known velocity, or we can accurately measure the velocity of a target with known range. However, if both parameters are unknown there is an ambiguous region in the τ, ω plane. For positive values of b, the ambiguous region lies in the first and third quadrants, as shown in Fig 10.13. Whether or not this ambiguity is important depends

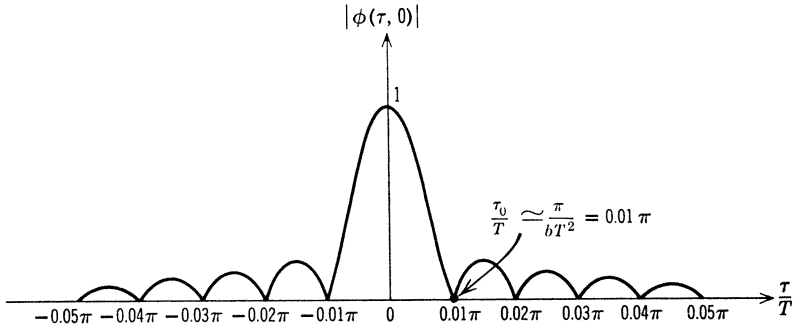

Fig. 10.14. Plot of $|\phi(\tau, 0)|$: rectangular pulse with linear *FM* ($bT^2 = 100$).

on the physical situation (i.e., can targets occur along this line in the τ, ω plane?). One way to resolve the ambiguity is to transmit a second pulse with the opposite frequency sweep.

A similar result follows for the rectangular pulse with a linear frequency modulation.

Example 5. Rectangular Pulse, Linear Frequency Modulation.

$$f(t) = \begin{cases} \frac{1}{\sqrt{T}} e^{jbt^2}, & -\frac{T}{2} \le t \le \frac{T}{2}, \\ 0, & \text{elsewhere.} \end{cases} \tag{52}$$

Using (23) and (42b), we have

$$|\phi(\tau, \omega)| = \begin{cases} \left(1 - \frac{|\tau|}{T}\right) \left| \frac{\sin\left(((\omega - 2b\tau)/2)(T - |\tau|)\right)}{((\omega - 2b\tau)/2)(T - |\tau|)} \right|, & \tau \le T, \\ 0, & \text{elsewhere.} \end{cases} \tag{53}$$

Along the τ-axis,

$$|\phi(\tau, 0)| = \begin{cases} \left(1 - \frac{|\tau|}{T}\right) \frac{\sin\left[b\tau(T - |\tau|)\right]}{b\tau(T - |\tau|)}, & |\tau| < T, \\ 0, & \text{elsewhere.} \end{cases} \tag{54}$$

Along the ω-axis,

$$|\phi(0, \omega)| = \left| \frac{\sin(\omega T/2)}{\omega T/2} \right|. \tag{55}$$

In Fig. 10.14, we have plotted $|\phi(\tau, 0)|$ for the case when $bT^2 = 100$. We see that the first zero is near the point

$$\tau_0 = \frac{T}{2}\left[1 - \left(1 - \frac{4\pi}{bT^2}\right)^{\frac{1}{2}}\right] \simeq \frac{\pi}{bT} = \frac{1}{W_0}, \tag{56}$$

where

$$2\pi W_0 \triangleq 2bT \tag{57}$$

is the range of the frequency sweep. Thus, as we would expect from our discussion of the Gaussian pulse, the range estimation accuracy for a known velocity target is proportional to the signal bandwidth. Once again there is a region of ambiguity in the first and third quadrants for positive b.

The performance of the receiver for Example 5 has an interesting interpretation. The input is the "long" pulse shown in Fig. 10.15*a*. Its instantaneous frequency increases with time, as shown in Fig. 10.15*b*. Now, the transfer function of the matched filter has a phase characteristic that is quadratic with respect to frequency. The delay of the envelope of a bandpass signal through any filter is proportional to the derivative of the

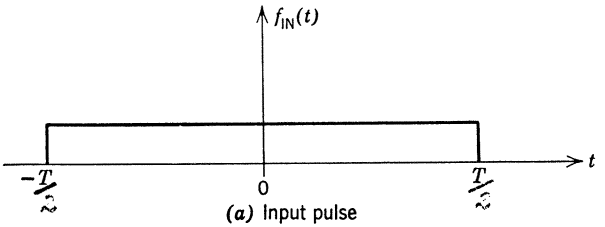

(a) Input pulse

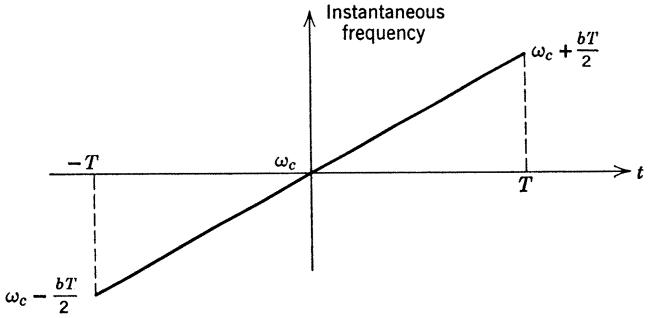

(b) Frequency characteristic

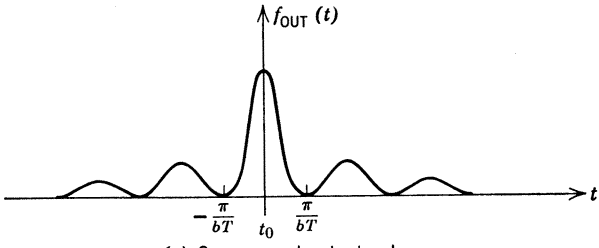

(c) Compressed output pulse

Fig. 10.15 Pulse compression.

phase characteristic of the filter with respect to frequency (e.g., [2]. For the linear *FM* pulse, the derivative of the phase of the matched filter decreases linearly with increasing frequency. Thus, the low-frequency components, which occur at the beginning, are delayed more than the high-frequency-components at the end of the pulse. The result is the "short" pulse shown in Fig. 10.15*c*. The effect of the receiver is to compress the long pulse at the input to the receiver into a short pulse at the output of the processor, with an accompanying increase in range measurement accuracy. This type of system is commonly referred to as a "*pulse-compression*" *radar*. Its obvious advantage is that if the system is peak-power-limited, one can increase the *transmitted energy* by transmitting a longer pulse without losing range accuracy. The idea of pulse compression through the use of frequency modulation was derived independently in the United States (Dicke [3] and Darlington [4]) and in Germany (Huttman [5] and Cauer [6]). An interesting discussion is given by Cook [7].

This series of examples illustrates the fundamental role that the ambiguity function plays in the range-Doppler estimation problem. We now return to the general case and derive some quantitative performance results. In Section 10.2, we derive expressions for the estimation accuracies in terms of the ambiguity function. In Section 10.3, we develop some general properties of the ambiguity function. Then, in Section 10.4, we return to signal design problems.

10.2 PERFORMANCE OF THE OPTIMUM ESTIMATOR

In this section, we discuss the accuracy of our estimates of τ and ω. We first consider the case in which the energy-to-noise ratio is high and the errors are small. We refer to this as the *local accuracy* problem.

The accuracy problem for range measurement was studied by Woodward [60]. The accuracy problem for range and velocity measurement has been studied by Manasse [76] and by Kelly, Reed, and Root [77].

10.2.1 Local Accuracy

We approach the local accuracy problem in two steps. First, we derive the Cramér-Rao bound on the accuracy of any unbiased estimates. We then argue that the errors using maximum likelihood estimates approach these bounds under certain conditions. We discuss these conditions in detail in Section 10.2.2.

The derivation of the Cramér-Rao bound is a straightforward application of the techniques in Sections I-4.2.3 and I-4.6. We recall that the first

step was to derive an *information matrix* **J** whose elements are

$$J_{ij} = -E\left[\frac{\partial^2 \ln \Lambda(\mathbf{A})}{\partial A_i \, \partial A_j}\right] \tag{58}$$

(see page I-372). In this case the parameters of interest, τ and ω, are nonrandom, so that the expectation is over $r(t)$ [or $n(t)$]. Here the information matrix is two-dimensional:

$$\mathbf{J} = \begin{bmatrix} J_{11} & J_{12} \\ J_{21} & J_{22} \end{bmatrix}. \tag{59}$$

We identify the subscript 1 with τ and the subscript 2 with ω. From (6), (58), and (59),

$$J_{11} = -E\left[\frac{\partial^2 \ln \Lambda_1(\tau, \omega)}{\partial \tau^2}\right], \tag{60}$$

$$J_{22} = -E\left[\frac{\partial^2 \ln \Lambda_1(\tau, \omega)}{\partial \omega^2}\right], \tag{61}$$

$$J_{12} = J_{21} = -E\left[\frac{\partial^2 \ln \Lambda_1(\tau, \omega)}{\partial \tau \, \partial \omega}\right]. \tag{62}$$

The evaluation of these three quantities is a straightforward manipulation. We shall state the results first and then carry out the derivation. The elements of the information matrix are

$$J_{11} = C[\overline{\omega^2} - (\bar{\omega})^2] = C\sigma_\omega^2, \tag{63}$$

and

$$J_{12} = C[\overline{\omega t} - \bar{\omega}\bar{t}] = C\rho_{\omega t}, \tag{64}$$

$$J_{22} = C[\overline{t^2} - (\bar{t})^2] = C\sigma_t^2, \tag{65}$$

where

$$C \triangleq \frac{2\bar{E}_r}{N_0}\left(\frac{\bar{E}_r}{\bar{E}_r + N_0}\right) \tag{66}$$

and

$$\overline{\omega^2} = \int_{-\infty}^{\infty} \omega^2 |\tilde{F}(j\omega)|^2 \frac{d\omega}{2\pi}, \tag{67}$$

$$\overline{\omega t} \triangleq \operatorname{Im} \int_{-\infty}^{\infty} u\tilde{f}^*(u) \frac{\partial \tilde{f}^*(u)}{\partial u} \, du, \tag{68}$$

$$\overline{t^2} = \int_{-\infty}^{\infty} u^2 |\tilde{f}(u)|^2 \, du. \tag{69}$$

We assume that the quantities in (67)–(69) are finite.

We now carry out the derivation for a typical term and then return to discuss the implications.

Derivation of the terms in J. We consider J_{11} first. From (6),

$$\frac{\partial \ln \Lambda_1(\tau, \omega)}{\partial \tau} = C'\left[\tilde{L}(\tau, \omega)\frac{\partial \tilde{L}^*(\tau, \omega)}{\partial \tau} + \frac{\partial \tilde{L}(\tau, \omega)}{\partial \tau}\tilde{L}^*(\tau, \omega)\right]$$

$$= 2C' \operatorname{Re}\left[\tilde{L}(\tau, \omega)\frac{\partial \tilde{L}^*(\tau, \omega)}{\partial \tau}\right], \tag{70}$$

where

$$C' \triangleq \frac{1}{N_0}\frac{\bar{E}_r}{N_0 + \bar{E}_r}. \tag{71}$$

Differentiating again, we obtain

$$\frac{\partial^2 \ln \Lambda_1(\tau, \omega)}{\partial \tau^2} = 2C' \operatorname{Re}\left[\frac{\partial \tilde{L}(\tau, \omega)}{\partial \tau}\cdot\frac{\partial \tilde{L}^*(\tau, \omega)}{\partial \tau} + \tilde{L}(\tau, \omega)\frac{\partial^2 \tilde{L}^*(\tau, \omega)}{\partial \tau^2}\right]. \tag{72}$$

Similarly,

$$\frac{\partial^2 \ln \Lambda_1(\tau, \omega)}{\partial \tau\, \partial \omega} = 2C' \operatorname{Re}\left[\frac{\partial \tilde{L}(\tau, \omega)}{\partial \omega}\cdot\frac{\partial \tilde{L}^*(\tau, \omega)}{\partial \tau} + \tilde{L}(\tau, \omega)\frac{\partial^2 \tilde{L}^*(\tau, \omega)}{\partial \tau\, \partial \omega}\right] \tag{73}$$

and

$$\frac{\partial^2 \ln \Lambda_1(\tau, \omega)}{\partial \omega^2} = 2C' \operatorname{Re}\left[\frac{\partial \tilde{L}(\tau, \omega)}{\partial \omega}\frac{\partial \tilde{L}^*(\tau, \omega)}{\partial \omega} + \tilde{L}(\tau, \omega)\frac{\partial^2 L^*(\tau, \omega)}{\partial \omega^2}\right]. \tag{74}$$

Now recall from (7) that

$$\tilde{L}(\tau, \omega) = \int_{-\infty}^{\infty} \tilde{r}(t)\tilde{f}^*(t - \tau)\, e^{-j\omega t}\, dt. \tag{75}$$

Differentiating (75) twice with respect to τ and using the results in (70) and (72), we have

$$J_{11} = -E\left\{\frac{\partial^2 \ln \Lambda_1(\tau, \omega)}{\partial \tau^2}\right\}$$

$$= -2C'\left\{\int\int_{-\infty}^{\infty}\frac{\partial \tilde{f}^*(t - \tau)}{\partial \tau}\frac{\partial \tilde{f}(u - \tau)}{\partial \tau}\, e^{jw(t-u)}E[\tilde{r}(t)\tilde{r}^*(u)]\, dt\, du\right.$$

$$\left. + \int\int_{-\infty}^{\infty}\tilde{f}^*(t - \tau)\frac{\partial^2 \tilde{f}(u - \tau)}{\partial \tau^2}\, e^{jw(t-u)}E[\tilde{r}(t)\tilde{r}^*(u)]\, dt\, du\right\}. \tag{76}$$

The correlation function of $\tilde{r}(t)$ is

$$E[\tilde{r}(t)\tilde{r}^*(u)] = 2\sigma_b{}^2 E_t \tilde{f}(t - \tau)\tilde{f}^*(u - \tau)e^{jw(t-u)} + N_0\,\delta(t - u). \tag{77}$$

Substituting (77) into (76), we obtain

$$J_{11} = -2C'\left\{\bar{E}_r\left|\int_{-\infty}^{\infty}\frac{\partial\tilde{f}(t-\tau)}{\partial t}\tilde{f}^*(t-\tau)\,dt\right|^2 + N_0\int_{-\infty}^{\infty}\left|\frac{\partial\tilde{f}(t-\tau)}{\partial t}\right|^2 dt\right.$$
$$+ \operatorname{Re}\left[\bar{E}_r\int_{-\infty}^{\infty}|\tilde{f}(t-\tau)|^2\,dt\int_{-\infty}^{\infty}\frac{\partial^2\tilde{f}^*(u-\tau)}{\partial\tau^2}\tilde{f}(u-\tau)\,du\right]$$
$$\left.+ \operatorname{Re}\left[N_0\int_{-\infty}^{\infty}\tilde{f}(t-\tau)\frac{\partial^2\tilde{f}^*(t-\tau)}{\partial\tau^2}\,dt\right]\right\} \tag{78}$$

(Recall that $\bar{E}_r \triangleq 2\sigma_b{}^2E_t$.) We now simplify this expression by demonstrating that the first term is $(\bar{\omega})^2$ and that the sum of the second and fourth terms is zero. To do this, we first observe that

$$\int_{-\infty}^{\infty}|\tilde{f}(t-\tau)|^2\,dt = 1 \tag{79}$$

for all τ. In other words, the energy does not depend on the delay. Differentiating both sides of (79) with respect to τ, we have

$$\operatorname{Re}\left\{\int_{-\infty}^{\infty}\left[\frac{\partial\tilde{f}(t-\tau)}{\partial\tau}\tilde{f}^*(t-\tau)\right]dt\right\} = 0. \tag{80}$$

Differentiating again gives

$$\operatorname{Re}\left\{\int_{-\infty}^{\infty}\left(\frac{\partial^2\tilde{f}(t-\tau)}{\partial\tau^2}\tilde{f}^*(t-\tau) + \frac{\partial\tilde{f}(t-\tau)}{\partial\tau}\frac{\partial\tilde{f}^*(t-\tau)}{\partial\tau}\right)dt\right\} = 0. \tag{81}$$

Thus,

$$\operatorname{Re}\left[\int_{-\infty}^{\infty}\frac{\partial^2\tilde{f}^*(t-\tau)}{\partial\tau^2}\tilde{f}(t-\tau)\,dt\right] = -\int_{-\infty}^{\infty}\left|\frac{\partial\tilde{f}(t-\tau)}{\partial\tau}\right|^2 dt \tag{82}$$

Thus, the second term in (78) cancels the fourth term in (78).

Comparing the first term in (78) and the definition of $\bar{\omega}$ in the Appendix (A.16), and using Parseval's theorem, we see that the first term is $\bar{E}_r(\bar{\omega})^2$.

To simplify the third term, we use (79) and then observe that

$$\int_{-\infty}^{\infty}\left|\frac{\partial\tilde{f}(t-\tau)}{\partial\tau}\right|^2 dt = \int_{-\infty}^{\infty}\omega^2|\tilde{F}(\omega)|^2\frac{d\omega}{2\pi} = \overline{\omega^2}. \tag{83}$$

Using the above results in (78) gives

$$J_{11} = 2C'\bar{E}_r[\overline{\omega^2} - (\bar{\omega})^2], \tag{84}$$

which is (63). As pointed out in the Appendix, we usually choose the carrier so that

$$\bar{\omega} = 0. \tag{85}$$

The derivation of J_{12} and J_{22} is similar. (See Problem 10.2.1.)

The information matrix is specified by (63)–(66) as

$$\mathbf{J} = \frac{2\bar{E}_r}{N_0}\left(\frac{\bar{E}_r}{\bar{E}_r + N_0}\right)\begin{bmatrix}\overline{\omega^2} & \overline{\omega t}\\ \overline{\omega t} & \overline{t^2}\end{bmatrix}. \tag{86}$$

The information matrix is useful in two ways. If we denote the error covariance matrix for some pair of unbiased estimates as $\mathbf{\Lambda}_\varepsilon$,

$$\mathbf{J} - \mathbf{\Lambda}_\varepsilon^{-1} \tag{87}$$

is non-negative definite.

We now interpret this statement in relation to the maximum-likelihood-estimation procedure. When the joint probability density of the errors using *ML* estimation is Gaussian, this result has a simple interpretation. Denote the errors by the vector

$$\mathbf{a}_\varepsilon \triangleq \begin{bmatrix} \hat{\tau}_{ml} - \tau \\ \hat{\omega}_{ml} - \omega \end{bmatrix} \triangleq \begin{bmatrix} \tau_\varepsilon \\ \omega_\varepsilon \end{bmatrix}. \tag{88}$$

If $\mathbf{a}_\varepsilon$ has a Gaussian density, then

$$p_{\mathbf{a}\varepsilon}(\mathbf{A}_\varepsilon) = \frac{1}{2\pi |\mathbf{\Lambda}_\varepsilon|^{1/2}} \exp\left(-\frac{\mathbf{A}_\varepsilon^T \mathbf{\Lambda}_\varepsilon^{-1} \mathbf{A}_\varepsilon}{2}\right). \tag{89}$$

The equal-height contours are ellipses that are given by the equation

$$\mathbf{A}_\varepsilon \mathbf{\Lambda}_\varepsilon^{-1} \mathbf{A}_\varepsilon = k_i^2, \qquad i = 1, 2, \ldots \tag{90}$$

and are shown in Fig. 10.16. The result in (87) says that if we construct the bound ellipses,

$$\mathbf{A}_\varepsilon \mathbf{J} \mathbf{A}_\varepsilon = k_i^2, \tag{91}$$

they will lie wholly inside the actual ellipses. Since the probability of lying in the region outside an ellipse is e^{-k^2} (see page I-77), we can bound the actual probabilities.

In general, the errors do not have a Gaussian density. However, we shall show that under certain conditions, the *ML* estimates are unbiased and the probability density of the errors approaches a joint Gaussian density. (As we would expect, the Gaussian approximation is best near the mean of the density.)

The second way in which the information matrix is useful is to bound the variance of the individual errors. The variance of *any* unbiased estimate is bounded by the diagonal elements in $\mathbf{J}^{-1}$. Thus

$$\boxed{\text{Var}\,[\hat{\tau} - \tau] \geq \left[\frac{2\bar{E}_r}{N_0}\left(\frac{\bar{E}_r}{\bar{E}_r + N_0}\right)\right]^{-1}\left(\frac{\overline{t^2}}{\overline{\omega^2 t^2} - (\overline{\omega t})^2}\right)} \tag{92}$$

and

$$\boxed{\text{Var}\,[\hat{\omega} - \omega] \geq \left[\frac{2\bar{E}_r}{N_0}\left(\frac{\bar{E}_r}{\bar{E}_r + N_0}\right)\right]^{-1}\left[\frac{\overline{\omega^2}}{\overline{\omega^2 t^2} - (\overline{\omega t})^2}\right].} \tag{93}$$

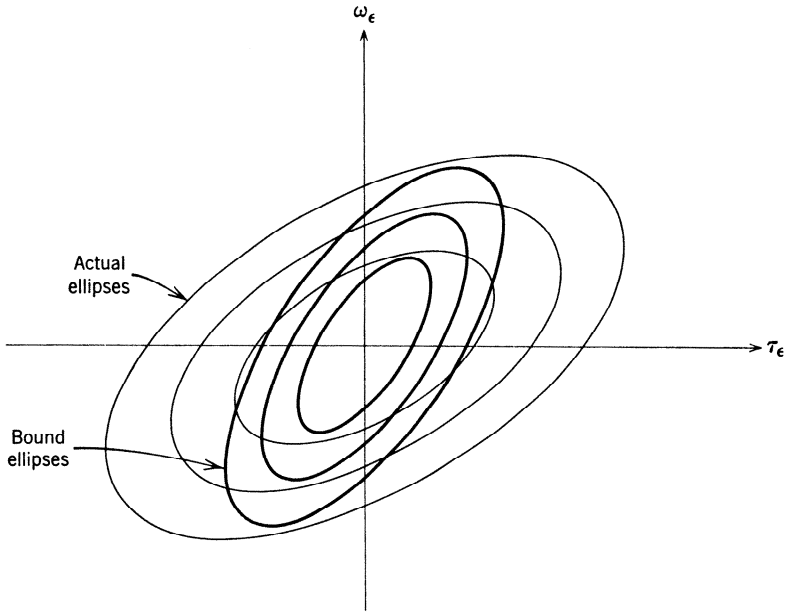

Fig. 10.16 Error ellipses.

Looking at (68), we see that a sufficient condition for the bounds on the estimation errors to be uncoupled is that the complex envelope be real. In this case,

$$\text{Var}\,[\hat{\tau} - \tau] \geq \left[\frac{2\bar{E}_r}{N_0}\left(\frac{\bar{E}_r}{\bar{E}_r + N_0}\right)\right]^{-1}\left[\frac{1}{\overline{\omega^2}}\right] \tag{94}$$

and

$$\text{Var}\,[\hat{\omega} - \omega] \geq \left[\frac{2\bar{E}_r}{N_0}\left(\frac{\bar{E}_r}{\bar{E}_r + N_0}\right)\right]^{-1}\left[\frac{1}{\overline{t^2}}\right] \tag{95}$$

for all *unbiased* estimates with $\overline{\omega t} = 0$. [Notice that (94) and (95) are bounds even with $\overline{\omega t} \neq 0$, but they are not as tight as (92) and (93).]

The first terms in (92)–(95) are functions of the ratio of the average received signal energy to the white noise level. The second terms indicate the effect of the signal shape. Looking at (94), we see that the bound on the delay estimation accuracy is determined by effective bandwidth. This is logical because, as we increase the signal bandwidth, we can design a signal with a faster rise time. From (95), we see that the bound on the Doppler estimation accuracy is determined by the effective pulse length.

Recalling the definition of the elements in the information matrix (60)–(62) and that of the ambiguity function, we would expect that the elements of **J** could be expressed directly in terms of the ambiguity function.

Property 2.† The elements in the matrix in (86) can be expressed as

$$\overline{\omega^2} - (\bar{\omega})^2 = -\frac{1}{2}\frac{\partial^2\theta(\tau, \omega)}{\partial\tau^2}\bigg|_{\omega,\tau=0}, \tag{96}$$

$$\overline{\omega t} - \bar{\omega}\bar{t} = -\frac{1}{2}\frac{\partial^2\theta(\tau, \omega)}{\partial\tau\,\partial\omega}\bigg|_{\omega,\tau=0}, \tag{97}$$

$$\overline{t^2} - (\bar{t})^2 = -\frac{1}{2}\frac{\partial^2\theta(\tau, \omega)}{\partial\omega^2}\bigg|_{\omega,\tau=0}. \tag{98}$$

These results follow from (17), (18) and (67)–(69) (see Problem 10.2.2).

Thus the information matrix can be expressed in terms of the behavior of the ambiguity function at the origin. Property 2 substantiates our intuitive observation on page 281 regarding desirable ambiguity functions.

The final step in our local accuracy discussion is to investigate when the actual estimation error variances approach the bounds given in (92) and (93). To motivate our discussion, we recall some results from our earlier work.

In our discussion of classical estimation theory on page I-71, we quoted some asymptotic properties of maximum likelihood estimates. They can be restated in the context of the present problem. Assume that we have N independent observations of the target. In other words, we receive

$$\tilde{r}_i(t) = \tilde{b}_i\sqrt{E_t}\,\tilde{f}(t - \tau)e^{j\omega t} + \tilde{w}_i(t), \qquad -\infty < t < \infty, \quad i = 1, 2, \ldots, N, \tag{99}$$

where the $\tilde{b}_i$ and $\tilde{w}_i(t)$ are characterized as in (3)–(5) and are statistically-independent. Physically this could be obtained by transmitting pulses at different times (the time-shift is suppressed in $\tilde{f}(t - \tau)$). Then, as $N \to \infty$,

1. The solution to the likelihood equation,

$$\frac{\partial \ln \Lambda_N(\tau, \omega)}{\partial\tau}\bigg|_{\substack{\tau=\hat{\tau}_{ml}\\ \omega=\hat{\omega}_{ml}}} = 0, \tag{100a}$$

$$\frac{\partial \ln \Lambda_N(\tau, \omega)}{\partial\omega}\bigg|_{\substack{\tau=\hat{\tau}_{ml}\\ \omega=\hat{\omega}_{ml}}} = 0, \tag{100b}$$

where

$$\ln \Lambda_N(\tau, \omega) = \sum_{i=1}^{N} \ln \Lambda_i(\tau, \omega), \tag{100c}$$

$$\ln \Lambda_i(\tau, \omega) = \frac{1}{N_0}\frac{\bar{E}_r}{N_0 + \bar{E}_r}\{|\tilde{L}_i(\tau, \omega)|^2\}, \tag{100d}$$

† We shall derive a number of properties of the ambiguity function in this chapter, and so we use a common numbering system for ease in reference.

and

$$\tilde{L}_i(\tau, \omega) \triangleq \int_{-\infty}^{\infty} \tilde{r}_i(t)\tilde{f}^*(t-\tau)e^{-j\omega t}\,dt, \tag{100e}$$

converges in probability to the correct value τ_a, ω_a as $N \to \infty$. Thus the *ML* estimates are consistent.

2. The *ML* estimates are efficient; that is

$$\lim_{N\to\infty} \frac{\text{Var}\,[\hat{\tau}_{ml} - \tau_a]}{\frac{1}{N}\left[\left(\frac{N_0}{2\bar{E}_r}\right)\left(\frac{\bar{E}_r + N_0}{\bar{E}_r}\right)\left(\frac{\overline{t^2}}{\overline{\omega^2 t^2} - \overline{(\omega t)^2}}\right)\right]} = 1, \tag{101}$$

and a similar relation for Var $[\hat{\omega}_{ml} - \omega_a]$.

3. The *ML* estimates are asymptotically jointly Gaussian with covariance matrix $\mathbf{J}^{-1}$.

These results relate to error behavior as the number of observations increase.

In Chapter I-4 (pages I-273 to I-287), we saw that the error variances approached the Cramér-Rao bound for large E/N_0. This is a different type of "asymptotic" behavior (asymptotic as $E/N_0 \to \infty$, not as $N \to \infty$.) In the present problem we would like to demonstrate that, using only one pulse, the error variance approaches the Cramér-Rao bound as $\bar{E}_r/N_0$ approaches infinity. Unfortunately, this does not seem to be true (see Problem 10.2.3). Thus the *ML* estimates are asymptotically efficient in the classical sense ($N \to \infty$) instead of in the high E/N_0 sense we encountered in Chapter 4.

There are two other issues concerning asymptotic behavior that should be mentioned:

1. Suppose that we use a fixed number of pulses, N (where $N > 1$) and let $\bar{E}_r/N_0$ increase. Do the error variances approach the bound? We have not been able to resolve this question to our satisfaction.

2. An alternative model that is sometimes used is

$$\tilde{r}(t) = \tilde{b}E_t\tilde{f}(t-\tau)e^{j\omega t} + \tilde{w}(t), \qquad -\infty < t < \infty, \tag{102a}$$

where $|\tilde{b}|$ is either a known amplitude or an unknown *nonrandom* amplitude. The local accuracy results [(58) to (69)] are valid for this model if we let

$$C \triangleq \frac{2E_t|\tilde{b}|^2}{N_0}, \tag{102b}$$

instead of using the value in (66). In this case we can show that the actual error variances approach the bounds as $C \to \infty$ (e.g., [77]).

All of our discussion in this section assumes that the errors are small. The next important question is the behavior of the errors when they are not small. We refer to this as the global accuracy (or ambiguity) problem.

10.2.2 Global Accuracy (or Ambiguity)

In this section we study the performance of the system when the errors are not necessarily small.

We can perform an approximate performance analysis by using the same technique as as in the *FM* threshold analysis on pages I-278–I-286.† The basic idea is straightforward. We assume that the region of the τ, ω plane that we must consider is a rectangle with dimensions Ω_* and T_*. We divide this region into rectangular cells, as shown in Fig. 10.17. The dimensions of the cell are proportional to the dimensions of the central peak of the signal ambiguity function. We shall use a grid with dimensions

$$\Delta_\tau = \frac{1}{\sigma_\omega} \tag{103a}$$

and

$$\Delta_\omega = \frac{1}{\sigma_t}, \tag{103b}$$

where

$$\sigma_t^2 = \overline{t^2} - (\bar{t})^2 \tag{103c}$$

and

$$\sigma_\omega^2 = \overline{\omega^2} - (\bar{\omega})^2. \tag{103d}$$

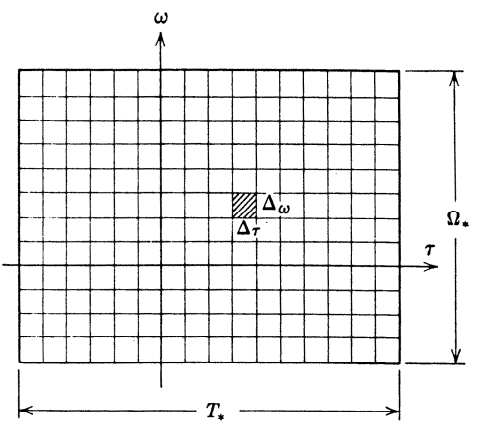

Fig. 10.17 Region in τ, ω plane in which targets may be present.

† We suggest that the reader review these pages, because our analysis in this section follows it closely.

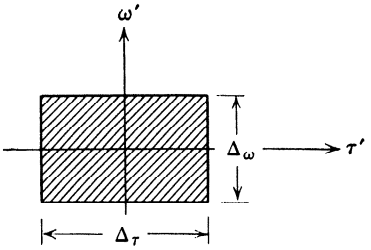

Fig. 10.18 Range-Doppler cell.

The cell is shown in Fig. 10.18. Notice that if $\overline{\omega t}$ is significant (e.g., in a linear *FM* signal) a parallelogram cell would be logical. We assume $\overline{\omega t}$ equals zero for simplicity.

We process the received signal in two steps. We first decide which of the cells the signal is in. We next perform a localization within the chosen cell. Thus, there are two kinds of errors: decision errors, because of picking the wrong cell, and local errors within the cell. The local errors were discussed in the last section. We now analyze the decision errors.

To analyze the errors we assume that the signal lies at the center of one of the cells. We denote the center point of the ith cell as (τ_i, ω_i). We assume that the a-priori probability that a signal will lie in any cell is equal. Thus we have an M-hypothesis problem where

$$M = \Omega_* \sigma_t T_* \sigma_\omega. \tag{104a}$$

The LRT consists of computing $|\tilde{L}_i|^2$,

$$|\tilde{L}_i|^2 = \left| \int_{-\infty}^{\infty} \tilde{r}(t) \tilde{f}^*(t - \tau_i) e^{-j\omega_i t}\, dt \right|^2, \tag{104b}$$

and choosing the largest. To analyze the performance, we must consider two cases.

Case 1. The signal ambiguity function has a central peak and no subsidiary peaks. The signal output in all incorrect cells is negligible.

Case 2. The signal ambiguity function has subsidiary peaks whose amplitudes are non-negligible.

We now analyze the first of these cases. The analysis for the second case is outlined briefly. The first case corresponds to transmitting one of M-orthogonal signals over a Rayleigh channel. The Pr (ϵ) for this case was derived in Problem I-4.4.24 (see also [I-80]).

For our purposes the approximate expression derived in Problem

I-4.4.25 (see also [I-90]) is most useful. The result is

$$\Pr(\epsilon) \simeq \frac{N_0}{\bar{E}_r}\left(\ln M - \frac{1}{2M} + 0.577\right). \tag{105}$$

As in Example 2 on page I-282, we can compute a mean-square error, given an interval error

$$E[\tau_\varepsilon^2 \mid \text{interval error}] \leq 2\sigma_{T_*}^2 = \frac{T_*^2}{6}, \tag{106a}$$

$$E[\omega_\varepsilon^2 \mid \text{interval error}] \leq 2\sigma_{\Omega_*}^2 = \frac{\Omega_*^2}{6}. \tag{106b}$$

In (106a) we have ignored the set of decision errors that cause no range error (i.e., choosing a cell at the correct range, but the wrong Doppler).

We now restrict our attention to the range estimation error. We can combine the various results to obtain an overall variance.

$$\begin{aligned} E(\tau_e^2) = {} & E(\tau_e^2 \mid \text{no decision error}) \Pr(\text{no decision error}) \\ & + E(\tau_e^2 \mid \text{decision error}) \Pr(\text{decision error}). \end{aligned} \tag{107a}$$

The only term that we have not evaluated is $E(\tau_e^2 \mid \text{no decision error})$. We can obtain a good approximation to this term, but it is too complicated for our present purposes. It is adequate to observe that the first term is nonnegative, so that the normalized error can be bounded by using only the second term. The result is

$$\begin{aligned} \frac{E(\tau_e^2)}{\text{Var}[T_*]} = \frac{E(\tau_e^2)}{T_*^2/12} &\geq \frac{12}{T_*^2} E(\tau_e^2 \mid \text{decision error}) \Pr(\text{decision error}) \\ &= \frac{2N_0}{\bar{E}_r}\left(\ln[\Omega_* \sigma_t T_* \sigma_\omega] - \frac{1}{2\Omega_* \sigma_t T_* \sigma_\omega} + 0.577\right). \end{aligned} \tag{107b}$$

From Section 10.2.1, we know that we also can bound the variance by using the Cramér-Rao bound. For large $\bar{E}_r/N_0$, the normalized Cramér-Rao bound is approximately

$$\frac{E(\tau_e^2)}{\text{Var}[T_*]} \geq \frac{N_0}{2\bar{E}_r} \frac{1}{(T_* \sigma_\omega)^2}. \tag{107c}$$

Comparing (107b) and (107c), we see that the right sides of both expressions have the same dependence on $\bar{E}_r/N_0$. However, for the parameter values of interest, the right side of (107b) is always appreciably larger than the right side of (107c). Thus, we conclude that, for a single transmitted pulse and a Rayleigh target model, the probability of a decision error dominates the error behavior, and we never achieve the variance indicated by the Cramér-Rao bound. The reason for this behavior is that in the

Rayleigh model we encounter targets with small $|\tilde{b}|^2$ regardless of how large $\bar{E}_r/N_0$ is. The large estimation errors associated with these small amplitude targets keep the average error from approaching the bound.

In Section 10.2.1, we indicated that the ML estimates were asymptotically efficient as the number of observations (that is, the number of pulses transmitted) approached infinity. We can now discuss the behavior as a function of N. For N pulses the Pr (ϵ) is approximately

$$\Pr(\epsilon) \simeq (\Omega_* \sigma_t T_* \sigma_\omega) \sqrt{\frac{1}{\pi N}} \frac{(1 + \bar{E}_r/N_0)^N}{(\bar{E}_r/N_0)(1 + \bar{E}_r/N_0)^{2N-1}} \tag{108a}$$

[use (I-2.516) and (I-4.64)]. If we assume that $E(\tau_e^2 \mid \text{no decision error})$ can be approximated by the right side of (92) then

$$\frac{E(\tau_e^2)}{\text{Var}\,[T_*]} \simeq \frac{1}{(T_* \sigma_\omega)^2} \frac{6}{N\bar{E}_r/N_0} \frac{1 + N\bar{E}_r/N_0}{N\bar{E}_r/N_0} (1 - \Pr(\epsilon)) + 2 \Pr(\epsilon). \tag{108b}$$

In Fig. 10.19, we have plotted the reciprocal of the normalized mean-square error as a function of N for various $\bar{E}_r/N_0$, $\Omega_* \sigma_t$, and $T_* \sigma_\omega$ values. As we would expect, there is a definite threshold effect. Below threshold the variance increases as $(\sigma_\omega T_*)(\sigma_t \Omega_*)$ is increased. Increasing $(\sigma_\omega T_*)(\sigma_t \Omega_*)$ also moves the threshold point to a larger value of N. Notice that even when $\bar{E}_r/N_0$ equals 10, it takes about 10 pulses to get above threshold.

In our discussion at the end of Section 10.2.1 we mentioned an alternative target model in which $|\tilde{b}|$ was modeled as a fixed quantity. It is interesting to discuss the global accuracy for this model. By a power series approach one can show that

$$E(\tau_e^2 \mid \text{no decision error}) = \frac{N_0}{2E_r} \frac{1}{\sigma_\omega^2}, \tag{109a}$$

where

$$E_r = E_t |\tilde{b}|^2, \tag{109b}$$

(see for example [77]). Using Problem 4.4.7 and (I-4.64),

$$\Pr(\epsilon) \leq \frac{\Omega_* \sigma_t T_* \sigma_\omega}{2} \exp\left(-\frac{E_r}{2N_0}\right). \tag{110}$$

Using (107a), (109), and (110), we obtain an expression for the normalized mean-square error. The reciprocal of the normalized mean-square error is plotted in Fig. 10.20 as a function of $E_r/2N_0$ for various values of $\Omega_* \sigma_t$ and $T_* \sigma_\omega$. Once again, we observe the threshold effect. Notice that if $(\sigma_\omega T_*)(\sigma_t \Omega_*)$ equals 10^4, then we need an E_r/N_0 of about 40 to get above threshold.

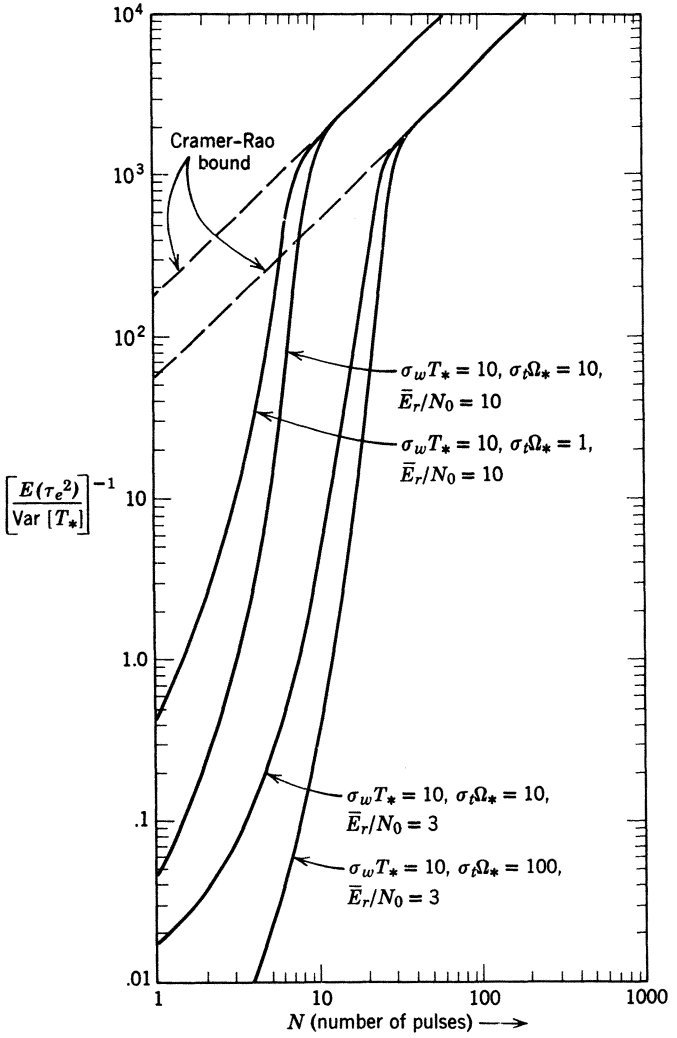

Fig. 10.19 Reciprocal of normalized mean-square error versus number of pulses: Rayleigh target model.

We should point out that in both Figs. 10.19 and 10.20, the location of the threshold is a function of the grid size that we selected. An analysis of the effect of grid size on the local and global errors could be carried out, but we have not done so.

All of our discussion up to this point has considered a signal whose ambiguity function had no subsidiary peaks. If the ambiguity function has subsidiary peaks, then the decision problem corresponds to the M-ary decision problem with nonorthogonal signals. For a particular signal

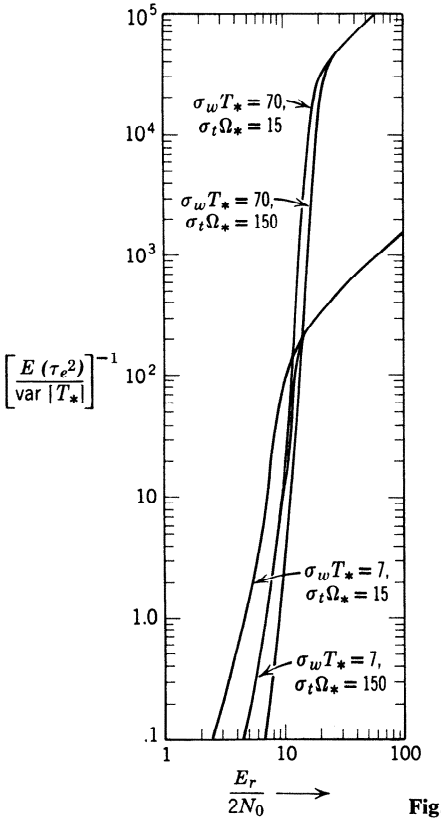

Fig. 10.20 Reciprocal of normalized mean-square error versus $E_r/2N_0$: nonfluctuating target model.

ambiguity function an approximate answer can be obtained, but the exact numerical results add little insight into the general case.

We should point out that there are other techniques available for studying the global accuracy problem. The Barankin bound discussed on pages I-71, I-147, and I-286 is quite useful (see for example [78]–[81]). Other references dealing with the global accuracy problem include [82]–[83].

10.2.3 Summary

In this section we have studied the performance of the optimum receiver. We have found that the local accuracy depends on the shape of the ambiguity function, $\theta(\tau, \omega)$, near the origin. We also studied the global accuracy (or ambiguity) problem. Here the performance depends on the behavior of $\theta(\tau, \omega)$ in the entire τ, ω plane.

Thus, we have established that in both the accuracy and ambiguity issues the functions $\phi(\tau, \omega)$ and $\theta(\tau, \omega)$ play a fundamental role. In the next section, we derive some useful properties of these functions.

10.3 PROPERTIES OF TIME-FREQUENCY AUTOCORRELATION FUNCTIONS AND AMBIGUITY FUNCTIONS

The autocorrelation and ambiguity functions were first introduced by Ville [1]. Their properties have been studied in detail by Woodward [8], Siebert [9], [10], Lerner [11], and Price [12].

The first property that we shall derive in this section concerns the volume under the ambiguity function. One implication of this property is that the ideal ambiguity function of Fig. 10.6 cannot exist.

Property 3 (Volume Invariance). The total volume under the ambiguity function is invariant to the choice of signal. Specifically,

$$\boxed{\int_{-\infty}^{\infty}\int_{-\infty}^{\infty} \theta(\tau, \omega)\, d\tau \frac{d\omega}{2\pi} = 1.} \tag{111}$$

Proof. The proof follows directly from the definitions in (17) and (18). We have

$$\iint_{-\infty}^{\infty} \theta(\tau, \omega)\, d\tau \frac{d\omega}{2\pi} = \int_{-\infty}^{\infty}\int_{-\infty}^{\infty}\int_{-\infty}^{\infty}\int_{-\infty}^{\infty} d\tau \frac{d\omega}{2\pi}\, dt\, du\, \tilde{f}\left(t - \frac{\tau}{2}\right)$$

$$\tilde{f}^*\left(t + \frac{\tau}{2}\right) e^{j\omega t} \tilde{f}^*\left(u - \frac{\tau}{2}\right) \tilde{f}\left(u + \frac{\tau}{2}\right) e^{-j\omega u}. \tag{112}$$

Integrating with respect to ω gives $2\pi\delta(t - u)$. Then integrating with respect to u changes u to t. This gives

$$\iint_{-\infty}^{\infty} \theta(\tau, \omega)\, d\tau \frac{d\omega}{2\pi} = \int_{-\infty}^{\infty}\int_{-\infty}^{\infty} d\tau\, dt \left|\tilde{f}\left(t - \frac{\tau}{2}\right)\right|^2 \left|\tilde{f}\left(t + \frac{\tau}{2}\right)\right|^2. \tag{113}$$

Let $z = t - (\tau/2)$. Then

$$\iint_{-\infty}^{\infty} \theta(\tau, \omega)\, d\tau \frac{d\omega}{2\pi} = \int_{-\infty}^{\infty} dz\, |\tilde{f}(z)|^2 \int_{-\infty}^{\infty} d\tau\, |\tilde{f}(\tau + z)|^2. \tag{114}$$

The inner integral equals unity for all z, since the energy is invariant to a time shift. The remaining integral equals unity, which is the desired result.

The implication of this result, which is frequently called the *radar uncertainty principle*, is clear. If we change the signal in order to narrow the main peak and improve the accuracy, we then must check to see where the displaced volume reappears in the τ, ω plane and check the effect on system performance. The radar uncertainty principle is probably the most important property of the ambiguity function. There are a number of other properties that are less fundamental but are useful in signal analysis and design.

The first group of properties deals principally with the time-frequency autocorrelation function (most of these were indicated in [10]). The proofs are all straightforward and many are left as exercises.

Property 4 (Symmetry).

$$\phi(\tau, \omega) = \phi^*(-\tau, -\omega) \tag{115}$$

and

$$\theta(\tau, \omega) = \theta(-\tau, -\omega). \tag{116}$$

Property 5 (Alternative Representations). An alternative representation of the time-frequency autocorrelation function is

$$\phi(\tau, \omega) = \frac{1}{2\pi} \int_{-\infty}^{\infty} \tilde{F}\left(j\alpha - \frac{j\omega}{2}\right) \tilde{F}^*\left(j\alpha + \frac{j\omega}{2}\right) e^{-j\alpha\tau}\, d\alpha. \tag{117}$$

At this point it is convenient to introduce a time-frequency autocorrelation function whose second argument is in cycles per second. We denote it by

$$\boxed{\phi\{\tau, f\} = \int_{-\infty}^{\infty} \tilde{f}\left(t - \frac{\tau}{2}\right) \tilde{f}^*\left(t + \frac{\tau}{2}\right) e^{j2\pi f t}\, dt.} \tag{118}$$

Similarly,

$$\theta\{\tau, f\} = |\phi\{\tau, f\}|^2. \tag{119}$$

The braces $\{\cdot\}$ indicate the definitions in (118) and (119), while the parentheses $(\cdot)$ indicate the original definition.†

Property 6 (Duality). The result in Property 5 points out an interesting duality that we shall exploit in detail later. Consider two signals, $\tilde{g}_1(t)$ and $\tilde{g}_2(t)$, such that

$$\tilde{g}_2\{f\} \triangleq \int_{-\infty}^{\infty} \tilde{g}_1(t) e^{-j2\pi f t}\, dt, \tag{120}$$

† We apologize for this diabolical notation. In most cases, the definition being used is obvious from the context and one can be careless. In duality problems one must be careful, because the definition cannot be inferred from the argument.

that is, $\tilde{g}_2\{\cdot\}$ is the Fourier transform of $\tilde{g}_1(\cdot)$. The result in (117) implies that

$$\phi_2\{f, -\tau\} = \phi_1\{\tau, f\}. \tag{121}$$

Thus the effect of transmitting the Fourier transform of a signal is to rotate the time-frequency diagram 90° in a *clockwise* direction.

Similarly,

$$\theta_2\{f, -\tau\} = \theta_1\{\tau, f\}. \tag{122}$$

Property 7 (Scaling). If

$$\tilde{f}(t) \sim \phi(\tau, \omega), \tag{123}$$

then

$$\sqrt{\alpha}\tilde{f}(\alpha t) \sim \phi\left(\alpha\tau, \frac{\omega}{\alpha}\right), \qquad \alpha > 0. \tag{124}$$

The ambiguity function is scaled in an identical manner.

Property 8. If

$$\tilde{F}(j\omega) \sim \phi(\tau, \omega), \tag{125}$$

then

$$\tilde{F}(j\omega)e^{j\alpha\omega} \sim \phi(\tau + 2\alpha\omega, \omega). \tag{126}$$

This is the frequency domain dual of Property 1 (page 290). The ambiguity function is changed in an identical manner.

Property 9 (Rotation). A generalization of the duality relation in Property 6 is the rotation property. Assume that

$$\tilde{f}_1(t) \sim \phi_1(\tau, \omega). \tag{127}$$

If we desire a new time-frequency function that is obtained by rotating the given $\phi_1(\cdot, \cdot)$, that is,

$$\phi_2(\tau, \omega) = \phi_1(\omega \sin\alpha + \tau\cos\alpha, \omega\cos\alpha - \tau\sin\alpha), \qquad 0 < \alpha < \frac{\pi}{2}, \tag{128}$$

we can obtain this by transmitting

$$\tilde{f}_2(t) = \frac{1}{\sqrt{\cos\alpha}} \exp\left(j\frac{t^2\tan\alpha}{2}\right) \int_{-\infty}^{\infty} \tilde{F}(j\omega) \exp\left(j\left(\frac{\omega^2\tan\alpha}{2} + \frac{\omega t}{\cos\alpha}\right)\right)\frac{d\omega}{2\pi}. \tag{129}$$

The ambiguity function is also rotated by α radians.

Property 10. A question of interest is: Given some function of two variables, $\phi\{\tau, f\}$, is it a time-frequency correlation function of some signal? We can answer this by taking the inverse transform of (118). Since

$$\phi\{\tau, f\} = \int_{-\infty}^{\infty} \tilde{f}\left(t - \frac{\tau}{2}\right) \tilde{f}^*\left(t + \frac{\tau}{2}\right) e^{j2\pi f t}\, dt, \tag{130}$$

$$\int_{-\infty}^{\infty} \phi\{\tau, f\} e^{-j2\pi f t}\, df = \tilde{f}\left(t - \frac{\tau}{2}\right) \tilde{f}^*\left(t + \frac{\tau}{2}\right). \tag{131}$$

Thus, if the transform of $\phi\{\tau, f\}$ can be written in the form shown in (131), it is a legitimate time-frequency correlation function and $\tilde{f}(t)$ is the corresponding signal. By a change of variables ($x = t - \tau/2$ and $y = t + \tau/2$), the relation in (131) can be rewritten as

$$\tilde{f}(x)\tilde{f}^*(y) = \int_{-\infty}^{\infty} \phi\{y - x, f\} \exp\left(-j2\pi f\left(\frac{x + y}{2}\right)\right) df. \tag{132}$$

By duality (Property 6), this can be written as

$$\tilde{F}\{x\}\tilde{F}^*\{y\} = \int_{-\infty}^{\infty} \phi\{f, x - y\} \exp\left(-j2\pi f\left(\frac{x + y}{2}\right)\right) df. \tag{133}$$

The relations in (132) and (133) enable us to determine the signal directly. Notice that the signal is unique except for a constant phase angle. Thus,

$$\tilde{f}_\alpha(x) \triangleq \tilde{f}(x) e^{j\alpha} \tag{134}$$

also satisfies (132).

A similar relation has not been derived for the ambiguity function. Thus, if we are given a function $\theta\{\tau, f\}$, we do not have a test that is both necessary and sufficient for $\theta\{\cdot, \cdot\}$ to be an ambiguity function. In addition, we do not have any direct procedure for finding an $\tilde{f}(t)$ that will produce a desired ambiguity function.

Property 11 (Multiplication). If

$$\tilde{f}_1(t) \sim \phi_1\{\tau, f\} \tag{135}$$

and

$$\tilde{f}_2(t) \sim \phi_2\{\tau, f\}, \tag{136}$$

then

$$\tilde{f}_1(t)\tilde{f}_2(t) \sim \int_{-\infty}^{\infty} \phi_1\{\tau, x\}\phi_2\{\tau, f - x\}\, dx \tag{137}$$

(i.e., convolution with respect to the frequency-variable), and

$$\tilde{F}_1\{f\}\tilde{F}_2\{f\} \sim \int_{-\infty}^{\infty} \phi_1\{x, f\}\phi_2\{\tau - x, f\}\, dx \tag{138}$$

(i.e., convolution with respect to the time variable).

Property 12 (Axis-Intercept Functions). The time-frequency correlation function evaluated at $\omega = 0$ is just the time-correlation function of the complex envelope,

$$\phi(\tau, 0) = \int_{-\infty}^{\infty} \tilde{f}\left(t - \frac{\tau}{2}\right) \tilde{f}^*\left(t + \frac{\tau}{2}\right) dt. \tag{139}$$

The time-frequency correlation evaluated at $\tau = 0$ has two interesting interpretations. It is the Fourier transform of the squared magnitude of the complex envelope,

$$\phi(0, \omega) = \int_{-\infty}^{\infty} |\tilde{f}(t)|^2 \, e^{j\omega t} \, dt. \tag{140}$$

From (117), it is the correlation function of the Fourier transform of the complex envelope,

$$\phi\{0, f\} = \int_{-\infty}^{\infty} \tilde{F}\left\{\left(x + \frac{f}{2}\right)\right\} \tilde{F}^*\left\{\left(x - \frac{f}{2}\right)\right\} df. \tag{141}$$

The final property of interest applies only to the ambiguity function.

Property 13 (Self-Transform). An ambiguity function is its own two-dimensional Fourier transform,

$$\int_{-\infty}^{\infty}\int \theta\{\tau, f\} \exp\left[j2\pi(vf - u\tau)\right] d\tau \, df = \theta\{v, u\}. \tag{142}$$

Observe the sign convention in the definition of the double transform [minus on the time (first) variable and plus on the frequency (second) variable]. This choice is arbitrary and is made to agree with current radar/sonar literature. It is worth noting that the converse statement is not true; the self-transform property does not guarantee that a particular function is an ambiguity function.

In this section we have derived a number of useful properties of the time-frequency autocorrelation function and the ambiguity function. Several other properties are derived in the problems. In addition, the properties are applied to some typical examples.

Notice that we have not been able to find a necessary and sufficient condition for a function to be an ambiguity function. Even if we know (or assume) that some two-variable function is an ambiguity function, we do not have an algorithm for finding the corresponding complex envelope. Thus, we can not simply choose a desired ambiguity function and then solve for the required signal. An alternative approach to the signal design problem is to look at certain classes of waveforms, develop the resulting

ambiguity function, and then choose the best waveform in the class. This is the approach that we shall use.

In Section 10.2, we examined modulated analog waveforms. We now look at a class of waveforms that we call coded pulse sequences.

10.4 CODED PULSE SEQUENCES

In this section we study complex envelopes consisting of a sequence of pulses that are amplitude-, phase-, and frequency-modulated. Each pulse in the sequence can be expressed as a delayed version of an elementary signal, $\tilde{u}(t)$, where

$$\tilde{u}(t) \triangleq \begin{cases} \dfrac{1}{\sqrt{T_s}}, & 0 \leq t \leq T_s, \\ 0, & \text{elsewhere.} \end{cases} \tag{143}$$

We denote the delayed version as $\tilde{u}_n(t)$,

$$\tilde{u}_n(t) \triangleq \tilde{u}(t - nT_s). \tag{144}$$

The complex envelope of interest is

$$\tilde{f}(t) = c \sum_{n=0}^{N-1} a_n \tilde{u}_n(t) \exp(j\omega_n t + j\theta_n). \tag{145}$$

We see that a_n is a constant amplitude modulation on the nth pulse, ω_n is a constant frequency modulation of the nth pulse, and θ_n is the phase modulation on the nth pulse. The constant c is used to normalize the envelope. The signal in (145) has $3N$ parameters that can be adjusted. We shall investigate the effect of various parameters.

Our discussion is divided into three parts:

1. A brief investigation of on-off sequences.
2. A development of a class of signals whose ambiguity functions are similar to the ideal ambiguity function of Fig. 10.6.
3. A brief commentary on other classes of signals that may be useful for particular applications.

10.4.1 On-off Sequences

The simplest example of an on-off sequence is the periodic pulse sequence in Example 3. Clearly, it can be written in the form of (145). To illustrate this, we assume that we have a periodic pulse sequence with interpulse spacing $T_p = 10T_s$ and a total of 10 pulses, as shown in Fig. 10.21. In the

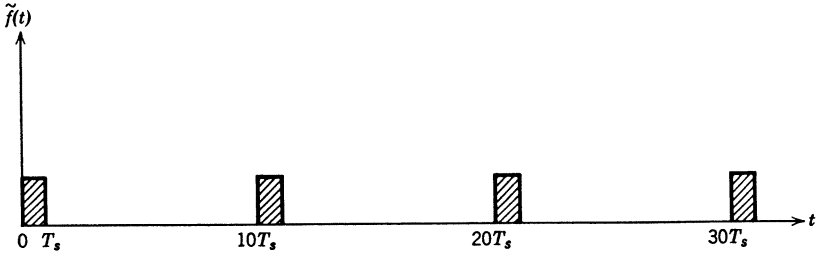

Fig. 10.21 Periodic pulse train.

notation of (145),

$$a_1 = a_{11} = a_{21} = \cdots a_{91} = 1, \tag{146}$$

and all other $a_n = 0$. Both ω_n and $\theta_n = 0$ for all n.

The disadvantage of the periodic sequence was the presence of large subsidiary peaks in the ambiguity function. Since the peaks are caused by the periodic structure, we can try to eliminate them by using a non-uniform pulse-repetition rate. One way to construct such a sequence would be to have 100 possible pulse positions and insert 10 pulses randomly. This type of procedure has been investigated in detail (e.g., Rihaczek [13], Cook and Bernfeld [14, pages 232–240], Kaiteris and Rubin [15], and Resnick [16]). It can be shown (the easiest way is experimentally) that staggering the PRF causes a significant reduction in the sidelobe level. (A sidelobe is a subsidiary peak in the τ, ω plane.) The interested reader can consult the above references for a detailed discussion.

10.4.2 Constant Power, Amplitude-modulated Waveforms

In this section, we consider the special case of (145) in which the waveforms can be written as

$$\tilde{f}(t) = c\sum_{i=1}^{N} a_n \tilde{u}_n(t), \tag{147}$$

where

$$a_n = \pm 1. \tag{148}$$

To motivate the use of this class of waveforms, let us recall the properties that an "ideal" ambiguity function should have:

1. The central peak should be narrow along the τ-axis. The minimum width of the central peak is governed by the signal bandwidth W. Here the bandwidth is the reciprocal of the length of the elemental pulse, T_s. Outside the region of the central peak, the ambiguity function should be

reasonably flat. From Property 12,

$$\phi(\tau, 0) = \int_{-\infty}^{\infty} \tilde{f}\left(t - \frac{\tau}{2}\right) \tilde{f}^*\left(t + \frac{\tau}{2}\right) dt. \tag{149}$$

Thus, we want a signal whose correlation function has the behavior shown in Fig. 10.22.

2. The central peak should be narrow along the ω-axis. From Property 12,

$$\phi(0, \omega) = \int_{-\infty}^{\infty} |\tilde{f}(t)|^2 e^{j\omega t} dt. \tag{150}$$

By making $|\tilde{f}(t)|$ constant over the entire signal sequence, we make $\phi(0, \omega)$ a narrow function of ω. This suggests choosing

$$a_n = \pm 1, \qquad n = 1, 2, \ldots, N. \tag{151}$$

Then

$$|\tilde{f}(t)| = \frac{1}{\sqrt{N}}, \qquad 0 \leq t < NT_s = T, \tag{152}$$

and the width on the f-axis is approximately $2/T$.

3. The ambiguity function should be reasonably flat except for the central peak. This requirement is harder to interpret in terms of a requirement on the signal. Therefore, we design signals using the first two requirements and check their behavior in the τ, ω plane to see if it is satisfactory.

4. The volume-invariance property indicates that if the ambiguity function is approximately flat away from the origin, its height must be such that the total volume integrates to unity. To compute this height, we observe that the total length of the ambiguity function is $2T$ if the duration of the complex envelope is T (recall $T = NT_s$). The ambiguity function does not have a finite width on the f-axis for a finite duration signal. However, we can approximate it by a width of $2W$ cycles per second, where W is the effective signal bandwidth. (In this case, $W = T_s^{-1}$.) With these approximations we have the desired ambiguity function shown in

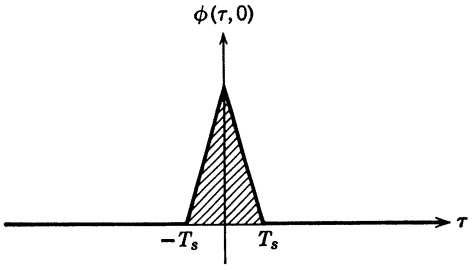

Fig. 10.22 A desirable signal correlation function.